ELSEVIER

Fluid Phase Equilibria 203 (2002) 141–176

FLUID PHASE EQUILIBRIA

www.elsevier.com/locate/fluid

A speciation-based model for mixed-solvent electrolyte systems

Peiming Wang*, Andrzej Anderko, Robert D. Young

OLI Systems Inc., 108 American Road, Morris Plains, NJ 07950, USA

Received 15 February 2002; accepted 7 June 2002

Abstract

A comprehensive model has been developed for the calculation of speciation, phase equilibria, enthalpies, heat capacities and densities in mixed-solvent electrolyte systems. The model incorporates chemical equilibria to account for chemical speciation in multiphase, multicomponent systems. For this purpose, the model combines standard-state thermochemical properties of solution species with an expression for the excess Gibbs energy. The excess Gibbs energy model incorporates a long-range electrostatic interaction term expressed by a Pitzer–Debye–Hückel equation, a short-range interaction term expressed by the UNIQUAC model and a middle-range, second virial coefficient-type term for the remaining ionic interactions. The standard-state properties are calculated by using the Helgeson–Kirkham–Flowers equation of state for species at infinite dilution in water and by constraining the model to reproduce the Gibbs energy of transfer between various solvents. The model is capable of accurately reproducing various types of experimental data for systems including aqueous electrolyte solutions ranging from infinite dilution to fused salts, electrolytes in organic or mixed, water + organic, solvents up to the solubility limit and acid–water mixtures in the full concentration range.

Keywords: Electrolytes; Mixed-solvent; Model; Excess properties; Gibbs energy of transfer; Speciation

1. Introduction

Electrolyte solutions are ubiquitous in numerous industrial processes and natural environments. Design and scale-up of unit operations in chemical process industries requires a thorough understanding of the chemical and phase behavior of process fluids. For example, design of separation processes (such as extractive distillation with salt or solution crystallization) requires a quantitative understanding of the effect of salts on phase behavior, prevention of corrosion requires the knowledge of chemical speciation in electrolyte solutions throughout a process, and environmental concerns require a precise control of the

* Corresponding author. Fax: +1-973-539-5922.
E-mail address: pwang@olisystems.com (P. Wang).

0378-3812/02/$ – see front matter
PII: S0378-3812(02)00178-4

concentrations of electrolytes in final products or in waste streams. These applications involve chemical systems that cover wide ranges of composition (aqueous, organic or mixed-solvent, dilute or concentrated solutions) and conditions (from ambient temperatures to supercritical conditions). Reliable models are, therefore, indispensable for predicting thermodynamic properties of electrolyte solutions, and the development of such models continues to be an important subject of research.

Numerous electrolyte solution models including those for mixed-solvent systems have been reported in the literature. In a recent paper [1], electrolyte solution models have been reviewed with emphasis on mixed-solvent systems. In general, three classes of models can be distinguished, i.e. models that treat electrolytes on an undissociated basis, those that assume complete dissociation of electrolytes into constituent ions and speciation-based models, which explicitly treat the solution chemistry. Although comparable results can be obtained for phase equilibrium calculations (especially VLE) with models that belong to various groups, speciation calculations become necessary whenever solution chemistry is sufficiently complex to manifest itself in thermodynamic properties. In mixed-solvents, ion pairing can be significant in comparison with aqueous environments due to the change of solvent properties such as a decrease in the dielectric constant. It is known that the degree of ion association varies substantially with solvent composition and the dielectric constant [2,3]. The change in ion association with composition can also be significant in common acids, such as the H_2O–HF and H_2O–H_2SO_4 mixtures. Speciation variations can also have a significant effect on phase equilibria, such as the solubility of salts, especially in multi-salt, mixed-solvent systems. In general, solution chemistry is an inherent part of the nonideality of electrolyte solutions and needs to be properly accounted for.

Mixtures of electrolytes and molecular solvents that are miscible at moderate temperatures from dilute electrolyte solutions to the fused salt limit are another important class of systems. Although relatively uncommon, they are of interest for both theoretical and practical reasons. The fused salt limit is becoming increasingly important in view of the interest in room-temperature ionic solvents. Thus, it is desirable to extend the definition of mixed-solvent electrolytes to include liquid salts and to develop thermodynamic models that are capable of reaching this limit.

In this work, we present a new, general, speciation-based thermodynamic model for mixed-solvent electrolyte systems. Here, the term “mixed-solvent electrolyte” encompasses systems of the following types:

1. aqueous electrolyte solutions from infinite dilution to fused salt;
2. fully miscible inorganic systems (e.g. H_2SO_4–water and HF–water) in a full concentration range;
3. electrolytes in organic or mixed organic + water solvents.

The model is designed to represent phase and chemical equilibria as well as thermal and volumetric properties in mixed-solvent electrolyte systems. The model is validated using experimental data on vapor–liquid equilibria, solubility, activities and activity coefficients, acid dissociation constants, Gibbs energies of transfer, heats of dilution and mixing, heat capacities, and densities.

2. Thermodynamic framework

The nonideality of an electrolyte solution arises from various forces including electrostatic (long-range) effects due to the electric charges of ionic species [4,5], chemical forces that lead to association or complex formation, physical dispersion forces and structural differences (e.g. in shape and relative size)

between species [6,7]. While the long-range forces predominate in dilute electrolyte solutions, the chemical and physical forces become increasingly important at moderate and short separation distances between species. The physical chemistry of electrolyte solutions becomes rather complex when all of these interactions occur simultaneously. To take into account the various effects, an expression for the excess Gibbs energy can be constructed as a sum of three terms:

$$\frac{G^{\mathrm{ex}}}{RT} = \frac{G^{\mathrm{ex}}_{\mathrm{LR}}}{RT} + \frac{G^{\mathrm{ex}}_{\mathrm{MR}}}{RT} + \frac{G^{\mathrm{ex}}_{\mathrm{SR}}}{RT} \tag{1}$$

where $G^{\mathrm{ex}}_{\mathrm{LR}}$ represents the contribution of long-range electrostatic interactions, $G^{\mathrm{ex}}_{\mathrm{SR}}$ is the short-range contribution resulting from molecule/molecule, molecule/ion, and ion/ion interactions, and an additional (middle-range) term $G^{\mathrm{ex}}_{\mathrm{MR}}$ accounts for ionic interactions (e.g. ion/ion and ion/molecule) that are not included in the long-range term. Similarly, the activity coefficient is given by

$$\ln \gamma_i = \ln \gamma_i^{\mathrm{LR}} + \ln \gamma_i^{\mathrm{MR}} + \ln \gamma_i^{\mathrm{SR}} \tag{2}$$

To account for speciation, the chemical effects due to the formation of ion pairs and complexes or the dissociation of these species can be explicitly expressed using chemical equilibria. Thus, for a chemical reaction:

$$aA + bB + \cdots = cC + dD + \cdots \tag{3}$$

the equilibrium conditions can be determined from

$$-\frac{\Delta G^{\circ}}{RT} = \ln\left(\frac{x_C^c x_D^d \cdots}{x_A^a x_B^b \cdots}\frac{\gamma_C^c \gamma_D^d \cdots}{\gamma_A^a \gamma_B^b \cdots}\right) \tag{4}$$

with

$$\Delta G^{\circ} = \sum_i \nu_i \mu_i^0 \tag{5}$$

where μ_i^0 is the standard-state chemical potential of species i, the sum is over all species participating in the chemical reaction, and ν_i is the stoichiometric coefficient of species i in Eq. (3) with positive values for the species on the right-hand side of the equation and negative values for those on the left-hand side. The algorithm for the determination of the chemical speciation in a mixed-solvent electrolyte system is similar to that used for aqueous solutions as described by Rafal et al. [8]. Thus, additional constraints, such as charge balance and the material balance, are used in the computation. For VLE calculations, the nonideality of the vapor phase can be conveniently modeled using a cubic equation of state such as the Soave–Redlich–Kwong (SRK) EOS.

Thus, the model presented in this work combines an expression for the excess Gibbs energy with chemical equilibrium relations that arise from ion association, complex formation, hydrolysis, etc.

2.1. Reference state

An important issue in modeling electrolyte solutions is the selection of a reference state. For the long-range electrostatic interaction term, the commonly used expression is that originally developed by Debye and Hückel [4]. The Debye–Hückel theory was originally developed in the McMillan–Mayer framework where the solvent appears only as a dielectric continuum, and the ionic reference state is always at infinite dilution in the dielectric medium. In general, such an unsymmetrical reference state

depends on the composition of the solvent mixture. On the other hand, the excess Gibbs energy models used to represent the short-range interactions, such as NRTL and UNIQUAC, use the pure liquid at the system temperature and pressure as the reference state. Thus, in modeling mixed-solvent electrolyte solutions, different reference states are generally used for ionic species and for solvents, i.e. the infinite dilution state in pure water or in a mixed-solvent has been used as the reference state for ions, and the pure liquid is commonly used as the reference state for solvents [9–16]. In addition, concentration units used in some of these models are different for the electrolytes and for the solvents. Commonly, molality is used for the electrolyte or "solute", and mole fraction is used for the "solvent" [9–12,14,16]. The use of molality does not allow the model to be extended to very concentrated electrolytes that approach fused salts or pure acids. In some models, in which the long-range interaction contribution has been neglected [17,18], a symmetrical reference system is used for all components (i.e. for both the solutes and solvents). This is justified by the fact that the effect of long-range electrostatic interactions on phase equilibria is negligible for electrolyte concentrations sufficiently remote from infinite dilution [19,20]. It has been noted [18,21] that an inconsistency may occur in solubility and liquid–liquid equilibrium (LLE) calculations with models that use different reference states for ions and solvents unless the standard state of the ionic species is properly selected [21]. In addition, a reference state based on the infinite dilution in water limits the applicability of the model to water-dominated systems. On the other hand, models that neglect the long-range interaction contribution and use the symmetrical convention for all components do not show the correct limiting behavior according to the Debye–Hückel theory and are not suitable for chemical equilibrium calculations because the electrolyte is assumed to be undissociated [17–19].

In view of the necessity to perform speciation calculations and in order to make the model applicable over wide ranges of compositions, the symmetrical reference state has been selected in the present work. Thus, for any of the three contributions to the excess Gibbs energy, the activity coefficient is normalized to the unit mole fraction, i.e. $\gamma_i = 1$ as $x_i \rightarrow 1$ for all of the species. Obviously, such a reference state is hypothetical for ions. The symmetrical reference state makes no distinction between the "solvent" and the "solute". This is especially convenient when modeling thermodynamic properties of liquid mixtures of any composition, e.g. electrolyte solutions from infinite dilution to fused salts or acids or nonelectrolyte mixtures in full concentration ranges. The concentration unit in the model is mole fraction for all species.

2.2. Standard-state chemical potentials

As discussed above, speciation calculations require the use of standard-state chemical potentials, μ_i^0, for all species that participate in a chemical reaction. For electrolyte solutions, the standard-state chemical potential can be generally based on the following conventions: (1) infinite dilution in water on the molality scale (unsymmetrically normalized, $\mu_i^{*,m,0}$, where "$*$" in the superscript denotes infinite dilution with respect to water); (2) infinite dilution in water on the mole fraction scale (unsymmetrically normalized, $\mu_i^{*,x,0}$); (3) pure component on the mole fraction scale (symmetrically normalized, $\mu_i^{x,0}$). Thermochemical data for aqueous species are available from extensive thermodynamic databases [8], and the temperature and pressure dependence of the standard-state properties can be calculated using a comprehensive model developed by Helgeson and coworkers (commonly referred to as the Helgeson–Kirkham–Flowers equation of state [22–25]). The parameters of this model are available for a large number of aqueous species including ions, associated ion pairs, and neutral species (inorganic and organic) [26–30]. These standard-state property data, which provide a basis for speciation calculations, are based on the infinite dilution in water reference state and on the molality concentration scale. When combined with

symmetrically-normalized activity coefficients for speciation calculations, these standard-state properties need to be appropriately converted. Conversion of the standard-state chemical potentials among the three reference states can be performed on the basis of an activity coefficient model [31]. In addition, due to the change of the solvent from water to a solvent mixture, the Gibbs energy of transfer of the electrolyte must be correctly accounted for to ensure the correctness of the chemical potentials in the mixed-solvent for speciation calculations. The conversion of the standard-state chemical potentials and the inherent thermodynamic consistency issues will be discussed in Sections 2.6 and 2.7. Analogous conversions for the standard-state enthalpy and volume calculations will be discussed in Sections 2.8 and 2.9.

2.3. Long-range interaction contribution

Various Debye–Hückel-type excess Gibbs energy expressions have been proposed in the literature to represent the long-range electrostatic interactions between ions at low electrolyte concentrations. The extended form proposed by Pitzer [32,33] has been most satisfactory in empirical tests, and has been used for modeling aqueous electrolyte solutions from infinite dilution to the fused salt limit [34–37] as well as for mixed-solvent electrolyte systems [15,38,39]. Thus, because of its empirical effectiveness, the Pitzer–Debye–Hückel expression is used for the long-range electrostatic contribution in this study. When normalized to mole fractions of unity for any pure species, the Pitzer–Debye–Hückel expression for the excess Gibbs energy is written as:

$$\frac{G^{\mathrm{ex}}_{\mathrm{DH}}}{RT} = -\left(\sum_i n_i\right)\frac{4A_x I_x}{\rho}\ln\left(\frac{1+\rho I_x^{1/2}}{\sum_i x_i[1+\rho(I^0_{x,i})^{1/2}]}\right) \tag{6}$$

where the sum is over all of the species (ionic and neutral) and I_x is the mole fraction-based ionic strength defined by

$$I_x = -\frac{1}{2}\sum_i x_i z_i^2 \tag{7}$$

$I^0_{x,i}$ represents the ionic strength when the system composition reduces to a pure component i, i.e. $I^0_{x,i} = (1/2)\, z_i^2$, ρ is related to a hard-core collision diameter and is treated as an empirical constant [34,40]. A value of $\rho = 14.0$ is used in this study. The A_x parameter is given by

$$A_x = \frac{1}{3}(2\pi N_{\mathrm{A}} d_{\mathrm{s}})^{1/2}\left(\frac{e^2}{4\pi\varepsilon_0\varepsilon_{\mathrm{s}}k_{\mathrm{B}}T}\right)^{3/2} \tag{8}$$

where N_{A} is the Avogadro number ($6.022137\times10^{23}\,\mathrm{mol}^{-1}$), d_{s} the molar density of the solution ($\mathrm{mol\,m}^{-3}$), e the electron charge ($1.602177\times10^{-19}\,\mathrm{C}$), $\pi = 3.14159$, ε_0 the permittivity of vacuum ($8.8541878\times10^{-12}\,\mathrm{C^2\,J^{-1}\,m^{-1}}$), ε_{s} the dielectric constant, k_{B} the Boltzmann constant ($1.38066\times10^{-23}\,\mathrm{J\,K^{-1}}$) and T is the temperature in K.

It has been long recognized from experimental evidence that there is a strong concentration dependence of the dielectric constant of ionic solutions [41]. However, for modeling water–organic–salt systems, the electrostatic interactions were usually represented by assuming no ionic concentration effect on the dielectric constant of water–organic mixtures [10–14]. The dielectric constants were also treated either as always equal to that of water [16,38] or as a constant [9,15]. For a more comprehensive representation of

the properties of mixed-solvent electrolyte systems, the effect of composition on the dielectric constant should be taken into account. A general model for the composition dependence of the dielectric constant has been developed in a previous paper [42] and has been used in this study to calculate ε_s in the Pitzer–Debye–Hückel long-range contribution term. By including this dielectric constant model, the long-range contribution reflects the electrostatic effects in the actual solution environment. Differentiation of Eq. (6) with respect to the number of moles at a constant temperature and pressure yields the following expression for the activity coefficient for any species k (ions and molecules):

$$\ln \gamma_k^{\mathrm{DH}} = -A_x \left[\frac{2z_k^2}{\rho} \ln \frac{1+\rho I_x^{1/2}}{\sum_i x_i [1+\rho (I_{x,i}^0)^{1/2}]} + \frac{I_x^{1/2}(z_k^2 - 2I_x)}{1+\rho I_x^{1/2}} \right] - \frac{4A_x I_x}{\rho} \left\{ \ln \frac{1+\rho I_x^{1/2}}{\sum_i x_i [1+\rho (I_{x,i}^0)^{1/2}]} \left(\sum_l n_l \right) \left[\frac{1}{2d_s} \frac{\partial d_s}{\partial n_k} - \frac{3}{2\varepsilon_s} \frac{\partial \varepsilon_s}{\partial n_k} \right] - \frac{1+\rho (I_{x,k}^0)^{1/2}}{\sum_i x_i [1+\rho (I_{x,i}^0)^{1/2}]} + 1 \right\} \tag{9}$$

It should be noted that the composition dependence of both density and the dielectric constant has been taken into account in the long-range interaction term. The sums in this expression cover all species.

2.4. Short-range interaction contribution

The short-range interaction contribution includes the interactions between all species. Local composition models originally developed for nonelectrolyte mixtures, such as the NRTL, Wilson, and UNIQUAC models, are appropriate for representing the short-range interactions in mixed-solvent electrolyte systems [9–12,14–16,38,39,43]. In this work, the UNIQUAC model [44] is selected for this purpose. The advantages of using UNIQUAC in representing short-range interactions are that: (1) its parameters often have a smaller temperature dependence compared to other models, which facilitates the use of fewer parameters when fitting data covering a wide temperature range; (2) it is applicable to solutions containing small or large molecules including polymers, because the primary concentration variable is the surface fraction, rather than the mole fraction [44]; (3) it can be extended to a group contribution framework, such as UNIFAC, to enhance the model's predictive capability.

The excess Gibbs energy in the UNIQUAC model is calculated as a sum of a combinatorial and a residual term [44]:

$$\frac{G_{\mathrm{UNIQUAC}}^{\mathrm{ex}}}{RT} = \frac{G_{\mathrm{combinatorial}}^{\mathrm{ex}}}{RT} + \frac{G_{\mathrm{residual}}^{\mathrm{ex}}}{RT} \tag{10}$$

with

$$\frac{G_{\mathrm{combinatorial}}^{\mathrm{ex}}}{RT} = \left(\sum_i n_i \right) \left[\sum_i x_i \ln \frac{\phi_i}{x_i} + \frac{Z}{2} \sum_i q_i x_i \ln \frac{\theta_i}{\phi_i} \right] \tag{11}$$

$$\frac{G_{\mathrm{residual}}^{\mathrm{ex}}}{RT} = -\left(\sum_i n_i \right) \left[\sum_i q_i x_i \ln \left(\sum_j \theta_j \tau_{ij} \right) \right] \tag{12}$$

$$\theta_i = \frac{q_i x_i}{\sum_j q_j x_j} \tag{13}$$

$$\phi_i = \frac{r_i x_i}{\sum_j r_j x_j} \tag{14}$$

$$\tau_{ji} = \exp\left(-\frac{a_{ji}}{RT}\right) \tag{15}$$

where q_i and r_i are the surface and size parameters, respectively, for the species i, Z a constant with a value of 10, a_{ij} the binary interaction parameter between species i and j ($a_{ij} \neq a_{ji}$). When applied to mixed-solvent electrolyte solutions, the subscripts i and j in these equations include all molecules (solvent molecules and undissociated electrolyte or neutral complexes) and ions. The activity coefficient equations that correspond to Eqs. (10)–(15) are given by Abrams and Prausnitz [44].

2.5. Middle-range interaction contribution

The middle-range term arises from interactions involving charged species (i.e. ion/ion and ion/molecule) that are not included in the long-range term. A symmetrical second virial coefficient-type expression is used to represent this contribution:

$$\frac{G^{\text{ex}}_{\text{MR}}}{RT} = -\left(\sum_i n_i\right)\sum_i\sum_j x_i x_j B_{ij}(I_x) \tag{16}$$

The quantity $B_{ij}(I_x)$ is a binary interaction parameter between the species i and j (ion or molecule) and is similar to the second virial coefficient representing the hard-core effects of charge interactions, which are found to be ionic strength-dependent [32]. The parameter $B_{ij}(I_x)$ has been assumed to be symmetric, i.e. $B_{ij}(I_x) = B_{ji}(I_x)$, and $B_{ii} = B_{jj} = 0$.

The activity coefficient is expressed as:

$$\ln \gamma_k^{\text{MR}} = \sum_i\sum_j x_i x_j B_{ij}(I_x) - \left(\sum_i n_i\right)\sum_i\sum_j x_i x_j \frac{\partial B_{ij}(I_x)}{\partial n_k} - 2\sum_i x_i B_{ik}(I_x) \tag{17}$$

2.6. Thermodynamic consistency in speciation calculations

As discussed in the beginning of this section, the computation of chemical equilibria requires the simultaneous use of activity coefficients and standard-state thermodynamic properties of all species participating in chemical reactions. Since the standard-state properties from the available thermodynamic databases [8] and the Helgeson–Kirkham–Flowers equation of state [26–30] are defined for infinite dilution in water on the molality basis, an appropriate conversion must be performed to make speciation calculations consistent when these properties are combined with the mole fraction-based, symmetrically-normalized activity coefficients. For this purpose, the mole fraction-based activity coefficient of species k in the symmetrical reference state, γ_k, is first converted to that based on the unsymmetrical reference state, i.e. at infinite dilution in water, γ_k^*, via

$$\ln \gamma_k^* = \ln \gamma_k - \lim_{\substack{x_k \to 0 \\ x_w \to 1}} \ln \gamma_k \tag{18}$$

where $\lim_{\substack{x_k\to 0\\ x_w\to 1}} \ln \gamma_k$ is the value of the symmetrically-normalized activity coefficient at infinite dilution in water, which can be calculated by substituting $x_k = 0$ and $x_w = 1$ into the activity coefficient equations. At the same time, the unsymmetrical, molality-based standard-state chemical potential, $\mu_k^{*,m,0}$, can be converted to a mole fraction-based quantity, $\mu_k^{*,x,0}$, by

$$\mu_k^{*,x,0} = \mu_k^{*,m,0} + RT \ln \left(\frac{1000}{M_w} \right) \tag{19}$$

where M_w is the molar weight of water. The unsymmetrical activity coefficient based on Eq. (18) can then be used with the standard-state chemical potential calculated using Eq. (19) for chemical equilibrium calculations. It should be noted that this procedure remains valid even when the system of interest does not contain any water.

2.7. Standard Gibbs energy of transfer

As discussed above, the available extensive databases of thermochemical properties for aqueous species provide a foundation for modeling speciation in aqueous systems. When applied to speciation calculations in mixed-solvent electrolyte systems, the aqueous standard-state properties must be combined with accurately predicted Gibbs energies of transfer to ensure an accurate representation of chemical potentials. Thus, it is important for the activity coefficient model to reproduce the Gibbs energies of transfer. In a mixed-solvent electrolyte model, the change in the standard Gibbs energy of ions due to the change in the dielectric constant may be, in principle, accounted for by introducing a Born electrostatic solvation term. The Born term formally converts the reference state from infinite dilution in water to that in the mixed-solvent [15,21,45]. However, the Born term is not introduced in the present model. It has been found in this study that inclusion of the Born term does not contribute to the accuracy of the model. There are also indications in the literature that the Born term has been found to give inaccurate results when compared to experimental data [13]. In the present model, an accurate representation of the Gibbs energy of transfer is achieved by imposing constraints on the parameters of the activity coefficient model. For this purpose, we derive an expression to relate the Gibbs energy of transfer to the activity coefficients in aqueous and nonaqueous (or mixed-solvent) environments.

The Gibbs energy of transfer of ion i from solvent R to solvent S on a molal concentration (m) scale is defined as:

$$\Delta_{tr} G_i^{\circ}(R \to S)_m = \mu_i^{0,m,S} - \mu_i^{0,m,R} \tag{20}$$

where $\mu_i^{0,m,S}$ and $\mu_i^{0,m,R}$ are the standard-state (infinite dilution) chemical potentials of ion i in solvent S and R, respectively. Through appropriate thermodynamic manipulation, the standard-state chemical potential of ion i in solvent S can be related to that in water ($\mu_i^{*,m,0}$) and to the unsymmetrical (referenced to infinite dilution in water) activity coefficient, i.e.

$$\mu_i^{0,m,S} = \mu_i^{*,m,0} + RT \ln \left(\frac{1000}{M_w} \right) + RT \ln(x_i^S \gamma_i^{*,S}) - RT \ln m_i^S \tag{21}$$

where m_i^S and x_i^S are the molality and mole fraction, respectively, of ion i in solvent S, and $\gamma_i^{*,S}$ is the mole fraction-based unsymmetrical activity coefficient of ion i in solvent S, which can be calculated using

the excess Gibbs energy model described in previous sections. By substituting Eq. (21) into Eq. (20), a general expression is obtained:

$$\Delta_{\mathrm{tr}}G_i^{\circ}(R \rightarrow S)_m = RT\ln\frac{\gamma_i^{*,S}M_S}{\gamma_i^{*,R}M_R} \tag{22}$$

where M_S and M_R are the molecular weights of solvents S and R, respectively.[1] At infinite dilution, the Gibbs energy of transfer for an electrolyte C_cA_a from solvent R to S can be obtained by adding those of its constituent cation and anion. It should be noted that most published standard Gibbs energies of transfer are on the molar scale. Conversion of the standard Gibbs energy of transfer between the molar (M) and molal (m) scales is necessary for consistent calculations. This is made using the following expression [46]:

$$\Delta_{\mathrm{tr}}G^{\circ}_{C_cA_a}(R \rightarrow S)_M = \Delta_{\mathrm{tr}}G^{\circ}_{C_cA_a}(R \rightarrow S)_m + (c+a)RT\ln\left(\frac{\rho_R}{\rho_S}\right) \tag{23}$$

where ρ is the density of the designated solvent, and c and a are the stoichiometric coefficients of the cation and anion in the electrolyte.

2.8. Enthalpy and heat capacity calculations

As discussed above, the symmetrically-normalized activity coefficients are converted to unsymmetrical normalization in order to incorporate the available standard-state thermodynamic properties for consistent speciation calculations. A similar approach is adopted for enthalpy and heat capacity calculations. Thermal properties of mixtures are derived from the temperature derivative of the excess Gibbs energy. To be thermodynamically consistent, the enthalpies are also calculated based on the unsymmetrical normalization. Thus, the total enthalpy in the mixed-solvent electrolyte solution is:

$$h = \sum_i x_i h_i^* + h^{\mathrm{ex},*} \tag{24}$$

where h_i^* is the standard-state partial molar enthalpy of species i, which can be computed from the Helgeson–Kirkham–Flowers equation,[2] and $h^{\mathrm{ex},*}$ is the excess molar enthalpy of a mixed-solvent electrolyte solution. In the unsymmetrical normalization, $h^{\mathrm{ex},*}$ is expressed as:

$$h^{\mathrm{ex},*} = -RT^2\sum_i x_i\left(\frac{\partial\ln x_i}{\partial T}\right)_P - RT^2\sum_i x_i\left(\frac{\partial\ln\gamma_i^*}{\partial T}\right)_P \tag{25}$$

The first term in Eq. (25) arises from the variation of speciation with temperature due to the temperature dependence of the equilibrium constants. This term is introduced because speciation is taken into account in the model. The value of $h^{\mathrm{ex},*}$ differs from the excess molar enthalpy expressed in the symmetrical

[1] For mixed solvents, they are the weighted molar weights, i.e. $M_S = \sum_k x_k^S M_k$, where the sum is over all solvent components, x_k^S is the mole fraction of component k, and M_k is the molecular weight of k.

[2] It can be proved that $h_i^* = h_i^{*,m}$, i.e. the standard-state partial molar enthalpies are the same on the basis of both mole fraction and molality.

normalization, h^{ex}. The difference results from Eq. (18) and can be calculated as:

$$h^{ex} - h^{ex,*} = -RT^2 \sum_i x_i \left[\frac{\partial \ln(\lim \gamma_i)_{\substack{x_i \to 0 \\ x_w \to 1}}}{\partial T} \right]_{P,x} \tag{26}$$

Heat capacities can be found by differentiating the enthalpy equations (cf. Eqs. (24) and (25)) with respect to temperature.

Although thermodynamic properties such as standard-state partial molar enthalpies for organic components are available in aqueous thermochemical databases, they are typically determined based on experimental data in dilute aqueous solutions of these components. When a mixture contains a large amount of such organic components, the calculated thermodynamic properties may show large deviations from the experimental results due to the necessity of extrapolating the solution properties from infinite dilution. For systems that have a zero water content, the representation of organic-phase heat capacities becomes difficult using the unsymmetrically-normalized standard-state properties. Thus, the calculation of thermodynamic properties for a mixed-solvent electrolyte system must be constrained by the pure liquid properties for all components for which pure component data are available. Thus, a methodology has been developed to impose such constraints for thermal property calculations.

For the majority of organic compounds, pure liquid heat capacities, $C^0_{p,i}(T)$, have been determined as a function of temperature and are readily available [47]. They can be used to constrain the calculations of enthalpy and heat capacity in mixtures. First, the molar enthalpy of a pure liquid component, h^0_i, is calculated by integrating the heat capacity:

$$h^0_i = \int_{T_r}^{T} C^0_{p,i}(T)\, \mathrm{d}T \tag{27}$$

where T_r is a reference temperature at which the enthalpy of the pure liquid is set equal to zero. The values of h^0_i are the standard-state molar enthalpies in the symmetrical normalization, i.e.

$$h = \sum_i x_i h^0_i + h^{ex} \tag{28}$$

The value of h^0_i can be related to the standard-state partial molar enthalpy in the unsymmetrical normalization, h^*_i, by noting that the unsymmetrically and symmetrically-normalized standard-state chemical potentials are related by

$$\mu^*_i = \mu^0_i + RT \ln(\lim_{\substack{x_i \to 0 \\ x_w \to 1}} \gamma_i) \tag{29}$$

Therefore, differentiation with respect to temperature yields:

$$h^*_i = h^0_i - RT^2 \left[\frac{\partial \ln(\lim \gamma_i)_{\substack{x_i \to 0 \\ x_w \to 1}}}{\partial T} \right]_{P,x} \tag{30}$$

The value of h^*_i calculated from Eq. (30) for an organic component is then used in the enthalpy calculations (Eq. (24)). The values of h^*_i for other, especially ionic, species are obtained from the Helgeson–Kirkham–Flowers equation. Thus, the calculation of thermal properties has been constrained to reproduce the heat

capacities of pure liquid components. At the same time, properties for mixtures at other concentrations can also be accurately represented.

2.9. Density calculations

The methodology used for density calculations is similar to that used for thermal properties. The excess volume of mixed-solvent electrolyte solutions can be obtained by differentiating the excess Gibbs energy with respect to pressure. In the unsymmetrical convention, we obtain

$$v^{\mathrm{ex},*} = RT\sum_i x_i \left(\frac{\partial \ln \gamma_i^*}{\partial P}\right)_{T,x} \tag{31}$$

The volume of a mixture can be then found from

$$v = \sum_i x_i v_i^* + v^{\mathrm{ex},*} \tag{32}$$

where v_i^* is the standard-state partial molar volume of species i, which can be calculated from the Helgeson–Kirkham–Flowers equation for a variety of, mostly ionic, species.[3] In analogy to Eq. (30), the pure liquid molar volume of a species i, v_i^0, can be related to v_i^* by:

$$v_i^* = v_i^0 + RT\left[\frac{\partial \ln(\lim \gamma_i)_{x_i\to 0}^{x_w\to 1}}{\partial P}\right]_{T,x} \tag{33}$$

Thus, the calculation of the volumes (or densities) in mixed-solvent electrolyte solutions is constrained by the pure liquid volumes for most organic components and some inorganic components for which data are available [47]. The values of v_i^* and their temperature and pressure dependence for ionic species are calculated from the HKF model.

It should be mentioned that, while the standard-state properties (such as v_i^* and h_i^*) calculated from the Helgeson–Kirkham–Flowers model show divergences in the vicinity of the critical point of water due to the rapid changes in water compressibility, the current model is generally applicable in temperature ranges up to ca. $0.9 \times T_c$ of the solvent, which is outside of the region where the anomalous behavior of the standard-state properties occurs.

3. Evaluation of model parameters

The validation of the model and the evaluation of model parameters require a large amount of experimental data of various types. For this purpose, we used the compilations by Linke and Seidell [48], Stephen and Stephen [49], and Silcock [50] for solubility results; Maczynski and Skrzecz [51], Gmehling and Onken [52], Ohe [53] for vapor–liquid equilibrium data; Christensen et al. [54] for heat of mixing data and Handa and Benson [55] and Söhnel and Novotnỳ [56] for density data. The work of Marcus [46] provides a compilation of data for the standard molar thermodynamic properties of

[3] It can be proved that $v_i^* = v_i^{*,m}$, i.e. the standard-state partial molar volumes are the same on the basis of both mole fraction and molality.

ion solvation or transfer. Additional experimental data, especially those for the salt effects on VLE, solubility, density, heats of mixing and dilution, and heat capacities have been collected from original sources.

The types of experimental data used in the determination of model parameters include the following:

1. VLE data;
2. activity coefficients in completely dissociated aqueous systems (such as NaCl);
3. osmotic coefficients (or activity of water) in aqueous solutions;
4. solubility of salts in water, organic solvents and mixed-solvents;
5. acid dissociation constants as a function of solvent composition;
6. Gibbs energy of transfer of electrolytes;
7. densities;
8. heats of mixing and dilution;
9. heat capacities.

These experimental data cover the concentration ranges of $x = 0$–x_s (where x_s is the solubility of the salt) or $x = 0$–1, whichever applies, and temperatures up to 300 °C.

The adjustable parameters in the model are the binary interaction parameters in the UNIQUAC and the middle-range terms. These parameters are determined by simultaneous inclusion of all available experimental results of the above types in a single data regression run, and minimization of the differences between the experimental and calculated property values.

The structural parameters (surface area and size) in the UNIQUAC term for all nonelectrolyte components are based on Bondi's [57] normalized values [44] of van der Waals group volumes and surface areas. The values for ionic species are fixed to be 1.0. For inorganic neutral species, the surface and size parameters are assigned to be equal to those of water ($r = 0.92$; $q = 1.4$). For the UNIQUAC binary interaction parameters, a_{ij} and a_{ji}, a quadratic temperature dependence has been found, in most cases, satisfactory for fitting experimental data:

$$a_{ij} = a_{ij}^{(0)} + a_{ij}^{(1)} T + a_{ij}^{(2)} T^2 \tag{34}$$

For the middle-range term, the second virial coefficient-type parameters, $B_{ij}(I_x)$, for charge interactions (ion/ion, ion/molecule) are represented by an empirical expression:

$$B_{ij}(I_x) = b_{ij} + (c_{ij} + d_{ij} T) \exp(-\sqrt{I_x + a_1}) + e_{ij} T + f_{ij} T^2 \tag{35}$$

where b_{ij}, c_{ij}, d_{ij}, e_{ij}, and f_{ij} are adjustable parameters and a_1 is set equal to 0.01. The presence of the constant a_1 prevents the occurrence of an infinite value of $\partial B_{ij}(I_x)/\partial n_k$ at $I_x \to 0$ when Eq. (16) is differentiated to yield Eq. (17). The decrease of the second virial coefficient with ionic strength, which is embodied by Eq. (35), has been noted before [32]. In a statistical thermodynamic treatment of electrolyte solutions, Pitzer [32] derived a function of ionic strength that qualitatively describes the behavior of the second virial coefficient that arises from charge interactions as "short-range" effects (relative to the Debye–Hückel long-range effect). This function has provided a basis for the expressions for the second virial coefficient-type parameters [12,32]. The expression given in Eq. (35) varies with the ionic concentration in a way that is consistent with the trend described by Pitzer [32] and is adopted based on its effectiveness in fitting experimental data.

To model densities of mixed-solvent electrolyte solutions, additional adjustable parameters are introduced to include the pressure dependence in binary parameters. For this purpose, the following function

is used in the UNIQUAC term for representing densities at saturation pressures:

$$a_{ij} = (a_{ij}^{(3)} + a_{ij}^{(4)} T + a_{ij}^{(5)} T^2) P \tag{36}$$

The function for the pressure dependence of the middle-range parameter is:

$$\frac{\partial B_{ij}}{\partial P} = b'_{ij} + (c'_{ij} + d'_{ij} T)\exp(-\sqrt{I_x + a_1}) + [e'_{ij} + (f'_{ij} + g'_{ij} T)\exp(-\sqrt{I_x + a_1})]P + h'_{ij} P^2 \tag{37}$$

Here, the parameters, $a_{ij}^{(3)}$–$a_{ij}^{(5)}$ and b'_{ij}, c'_{ij}, d'_{ij}, e'_{ij}, f'_{ij}, g'_{ij}, h'_{ij} are determined separately from parameters that are used for phase equilibrium and enthalpy calculations (cf. Eqs. (34) and (35)). It should be noted that the complete model reduces to UNIQUAC for nonelectrolyte mixtures.

4. Results and discussions

The model has been validated using different types of experimental data for various classes of mixtures under wide ranges of conditions. The model can simultaneously reproduce VLE, activity coefficients, solubility, speciation in water and mixed-solvents, Gibbs energy of transfer of electrolytes, heats of dilution and mixing, heat capacities, and densities in electrolyte solutions ranging from infinite dilution in water to fused salts or pure acids. Table 1 lists the types of systems that have been examined in this work and the typical experimental data that were used to test the model. Parameters for selected systems are given in Table 2 to demonstrate the types of parameters required for various systems.

4.1. Modeling VLE and solubility in aqueous systems from dilute solutions to fused salts

Metal nitrates in water provide an example of systems that are continuously miscible from infinite dilution to the fused salt limit. These systems, for which extensive experimental data are available [58–63], provide good opportunities to examine the model in the full concentration range of the electrolyte component. VLE and solubility behavior for the ternary systems $AgNO_3$–$TlNO_3$–H_2O and $LiNO_3$–KNO_3–H_2O and all of their constituent binary subsystems (i.e. MNO_3–H_2O, M = Li, K, Ag, Tl) [58–63] have been examined in this study. Fig. 1 shows the VLE results for the $LiNO_3$–KNO_3–H_2O system at various temperatures. The solubilities of $LiNO_3$ and $AgNO_3$ in water at various temperatures are shown in Fig. 2. These results demonstrate that the model is capable of accurately representing the experimental results for aqueous electrolytes from dilute solutions to the limit of fused salts. Another example of simultaneous representation of VLE and solubility in aqueous systems is provided by the $CaCl_2$–H_2O system. The VLE results for this system are shown in Fig. 3 at various $CaCl_2$ concentrations. In Fig. 4, solubilities of various $CaCl_2$ hydrates are shown as a function temperature. In numerous industrial and geological applications, the solubility of compounds depends not only on temperature and solution composition, but also on the pressure of gaseous species such as CO_2. This is exemplified by the behavior of $CaCO_3$. Fig. 5 shows the results of solubility calculations for $CaCO_3$ in water at various temperatures as a function of the partial pressure of CO_2. The dependence of the solubility of $CaCO_3$ on temperature and P_{CO_2} has been accurately reproduced.

In addition to phase equilibria, the mean activity coefficients of completely dissociated electrolytes have also been used in calibrating the model. For example, activity coefficients in aqueous NaCl solutions at

Table 1
Types of systems studied and typical experimental data used in model validation

System	Examples	Concentration range	Types of data
Aqueous electrolyte systems			VLE, SLE, γ, H_{dil}, C_p, density
Salts with limited solubility	$NaCl–H_2O$		
	$CaCl_2–H_2O$	$x = 0–x_s$	
	$HCl–H_2O$		
Fully miscible acids	$HF–H_2O$		
	$H_2SO_4–H_2O$	$x = 0–1$	
	$HNO_3–H_2O$		
Salts miscible with water from dilute electrolyte to fused salts	$LiNO_3–KNO_3–H_2O$	$x = 0–1$	
	$NaOH–H_2O$		
Weakly dissociated systems			VLE, H_{mix}, C_p, density
	Methanol–H_2O		
	Acetic acid–H_2O	$x = 0–1$	
	Acetic acid–methanol		
Electrolytes in organic or mixed-solvents			VLE, SLE, $\Delta_{tr}G^\circ$, K_A, H_{mix}, C_p, density
	LiCl–methanol		
	HCl–methanol		
	$CaCl_2$–acetone–methanol		
	NaCl–methanol–H_2O		
	HCl–isopropanol–H_2O	$x = 0–x_s$	
	Acetic acid–ethanol–H_2O		

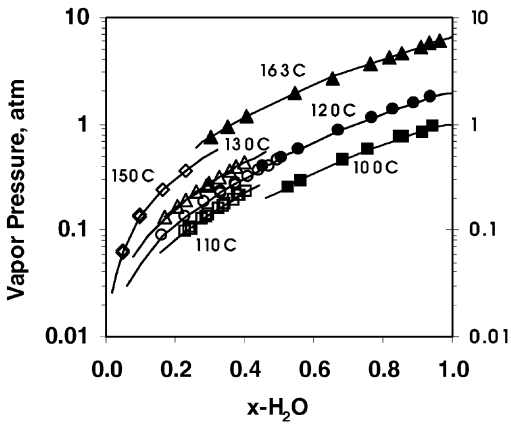

Fig. 1. Vapor pressure of the $LiNO_3–KNO_3–H_2O$ system at various temperatures (with the molar ratio Li/K = 1.0). The filled symbols are from Simonson and Pitzer [63], and the empty symbols are from Tripp [59] and Tripp and Braunstein [60]. The lines are calculated from the model.

Table 2
Parameters for representative systems

Systems	UNIQUAC parameters (Eq. (34))	Middle-range parameters (Eq. (35))	Experimental data sources
	$a^{(0)}_{H_2O,HCl_{aq}} = -148,301$ $a^{(1)}_{H_2O,HCl_{aq}} = 940.162$ $a^{(2)}_{H_2O,HCl_{aq}} = -1.21081$	$b_{H^+,Cl^-} = -139.738$ $c_{H^+,Cl^-} = 167.294$ $d_{H^+,Cl^-} = -0.427632$	[51,52,103, 118,119,120, 121]
HCl–water ($0 < T < 200\,^\circ C$)	$a^{(0)}_{HCl_{aq},H_2O} = 10,965.5$ $a^{(1)}_{HCl_{aq},H_2O} = -90.9743$	$e_{H^+,Cl^-} = 0.317799$ $f_{H^+,Cl^-} = 0.0$	
Isopropanol–water ($0 < T < 200\,^\circ C$)	$a^{(2)}_{HCl_{aq},H_2O} = 0.090474$	$b_{H^+,2\text{-PrOH}} = b_{Cl^-,2\text{-PrOH}} = 78.6504$	
HCl–isopropanol–water ($60 < T < 85\,^\circ C$)	$a^{(0)}_{H_2O,2\text{-PrOH}} = -4586.22$ $a^{(1)}_{H_2O,2\text{-PrOH}} = 11.7639$ $a^{(2)}_{H_2O,2\text{-PrOH}} = 0.00842474$ $a^{(0)}_{2\text{-PrOH},H_2O} = 4407.26$ $a^{(1)}_{2\text{-PrOH},H_2O} = 0.215586$ $a^{(2)}_{2\text{-PrOH},H_2O} = -0.0231173$	$c_{H^+,2\text{-PrOH}} = c_{Cl^-,2\text{-PrOH}} = -70.6361$ $d_{H^+,2\text{-PrOH}} = d_{Cl^-,2\text{-PrOH}} = 0.216608$ $e_{H^+,2\text{-PrOH}} = e_{Cl^-,2\text{-PrOH}} = -0.245043$ $f_{H^+,2\text{-PrOH}} = d_{Cl^-,2\text{-PrOH}} = 0$	
	$a^{(0)}_{Cl^-,Na^+} = -5550.83$ $a^{(1)}_{Cl^-,Na^+} = 19.9305$ $a^{(2)}_{Cl^-,Na^+} = -0.0735037$	$b_{Cl^-,Na^+} = -42.2615$ $c_{Cl^-,Na^+} = 41.8316$	[39,46,48, 51–54,103, 117,126–129, 133,134]
NaCl–water ($0 < T < 300\,^\circ C$)	$a^{(0)}_{Na^+,Cl^-} = -12,162.3$ $a^{(1)}_{Na^+,Cl^-} = 28.1739$	$d_{Cl^-,Na^+} = -0.0910231$ $e_{Cl^-,Na^+} = 0.0491386$	
Methanol–water ($-21 < T < 200\,^\circ C$)	$a^{(2)}_{Na^+,Cl^-} = -0.01196964$	$f_{Cl^-,Na^+} = 4.28128E-5$	
NaCl–methanol–water ($0 < T < 100\,^\circ C$)	$a^{(0)}_{H_2O,MeOH} = -3149.65$ $a^{(1)}_{H_2O,MeOH} = 24.4368$ $a^{(2)}_{H_2O,MeOH} = -0.0104692$ $a^{(0)}_{MeOH,H_2O} = -2799.16$ $a^{(1)}_{MeOH,H_2O} = 8.18056$ $a^{(2)}_{MeOH,H_2O} = -0.0194803$	$b_{Na^+,MeOH} = b_{Cl^-,MeOH} = -33.6701$ $c_{Na^+,MeOH} = c_{Cl^-,MeOH} = 32.8959$ $d_{Na^+,MeOH} = d_{Cl^-,MeOH} = -0.0787143$ $e_{Na^+,MeOH} = e_{Cl^-,MeOH} = 0.0909991$ $f_{Na^+,MeOH} = f_{Cl^-,MeOH} = -3.69465E-5$	

various temperatures are shown in Fig. 6. The mean activity coefficients of electrolytes in mixed-solvents such as in water–alcohol mixtures have been determined in a number of studies [64–68]. Customarily, the mean activity coefficient is defined based on the stoichiometric coefficients of the cation and anion assuming that the electrolyte completely dissociates. In mixed-solvents, however, due to the decrease in the dielectric constant, the dissociation may be incomplete, and the extent of ion pair formation depends on the composition of the solvent. The mean activity coefficients determined on the assumption of complete

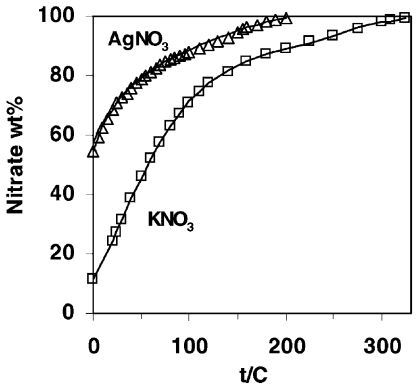

Fig. 2. Solubilities of $AgNO_3$ and KNO_3 as a function of temperature. The experimental data were taken from Linke and Seidell [48] and the lines were calculated from the model.

dissociation of electrolytes in a mixed-solvent will lead to an inconsistency when recalculated using a speciation model. Therefore, these data were not utilized in our study.

4.2. Modeling VLE and solubility in salt–mixed-solvent systems

In this section, we present the results of modeling VLE and solubility in systems containing salts, water and/or nonelectrolytes. In Fig. 7, the solubilities of NaCl in the methanol–H_2O and ethanol–H_2O mixtures at 25 °C are shown as a function of the alcohol mole fractions. VLE results are shown in Fig. 8 for the ethanol–H_2O–LiCl systems at 25 °C at two different LiCl concentrations. The salt-free VLE results are also shown in the figure. The "salting-out" effects can be accurately predicted as seen in the increase of the vapor phase mole fraction of the alcohol upon addition of the salt. Fig. 9 shows the results at saturated concentrations of $CaCl_2$ in acetone–methanol mixtures at 1.0 atm. Both the "salting-out" of acetone at

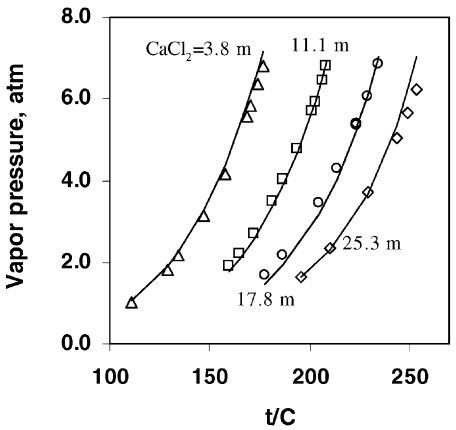

Fig. 3. Vapor pressure of the $CaCl_2$–H_2O system as a function of temperature at various $CaCl_2$ molalities. The experimental data were taken from Hoffmann and Viogt [113] and the lines were calculated from the model.

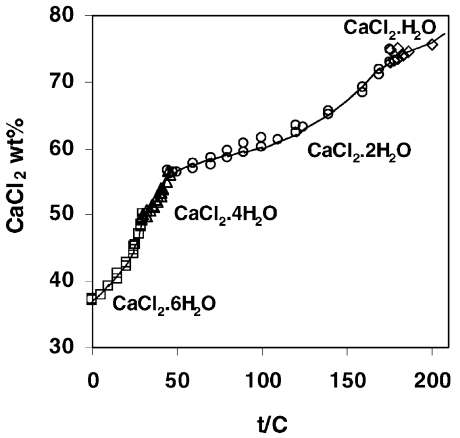

Fig. 4. Solubilities of various $CaCl_2$ hydrates in water as a function of temperature. The experimental data were taken from Linke and Seidell [48] and Garvin et al. [114]. The lines were calculated from the model.

high concentrations of methanol and the weak "salting-in" effect at low methanol concentrations can be accurately predicted. In the systems shown in these figures, the electrolytes have been assumed to completely dissociate and the weak dissociation of the alcohols has been taken into account using acid dissociation constants from the literature [68b].

The behavior of acids and bases in mixed-solvents is of particular interest in the study of solution properties that are dependent on pH. For example, due to changes in ionization, the corrosivity of an acid or a base may change significantly with the composition of the solution in which the metal is immersed. In

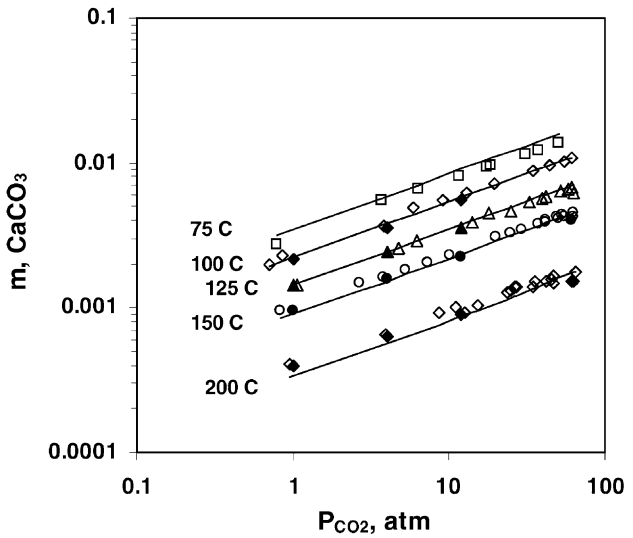

Fig. 5. Solubility of $CaCO_3$ in water at various temperatures as a function of P_{CO_2}. The lines were calculated using the model and the symbols are the experimental data from Signit et al. [115] (empty symbols) and Ellis [116] (filled symbols).

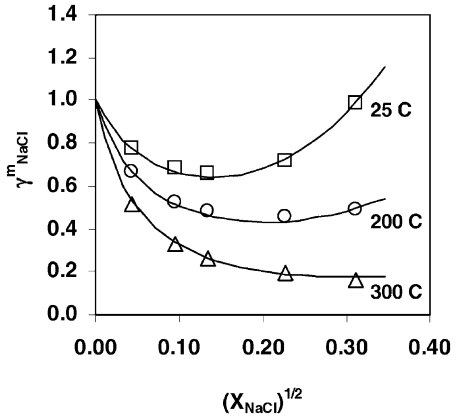

Fig. 6. The mean activity coefficients of NaCl in water at various temperatures. The symbols were taken from the smoothed values of Archer [117] and the lines were calculated from the model.

this work, systems containing acids in water and organic solvents were analyzed. The results of modeling VLE for the HCl–water and HCl–water–isopropanol systems are shown in Figs. 10 and 11. Fig. 10 shows VLE results for HCl–water at 0 and 70 °C. The results for the HCl–water–isopropanol system are shown in Fig. 11 at two compositions.

All of the results presented here show that the model can accurately reproduce experimental VLE and solubility data in salt–water–organic mixtures.

4.3. Modeling VLE and speciation in associating systems

Numerous industrial applications require the knowledge of the chemical speciation in electrolyte solutions. For example, speciation is of particular interest in the study of solution properties that are dependent

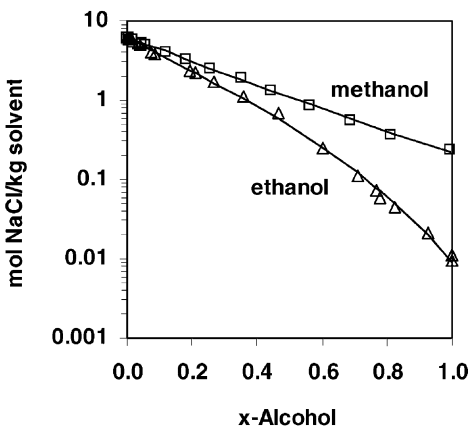

Fig. 7. Solubility of NaCl in methanol–water (upper curve) and ethanol–water (lower curve) mixtures at 25 °C. The experimental data were taken from Linke and Seidell [48] and Pinho and Macedo [39] and the lines were calculated from the model.

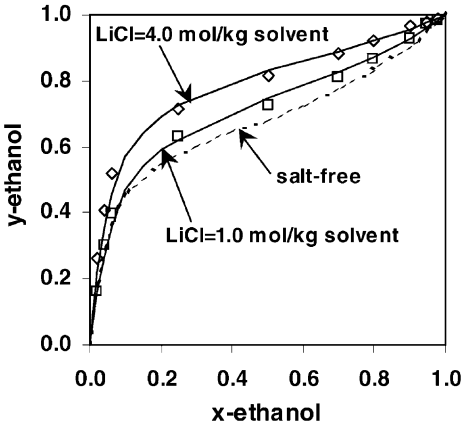

Fig. 8. VLE results for the LiCl–ethanol–water system at LiCl concentrations of 1.0 and 4.0 mol kg per solvent at 25 °C. The salt-free equilibria are also shown as a dashed line. Experimental data were taken from Ohe [53] and references cited therein. All lines were calculated using the model.

on pH, and in identifying the species that are responsible for certain phenomena such as corrosion or other electrochemical processes. Monoprotic acids such as formic and acetic acids in water–alcohol mixtures as well as the HF–H_2O and H_2SO_4–H_2O mixtures are among the systems that are characterized by moderate to strong ion association or polymerization. Extensive experimental VLE and thermal property data have been reported for these systems, and ionization constants for the monoprotic acids in water–alcohol mixtures are also available [2,3]. These data are convenient for testing the speciation model.

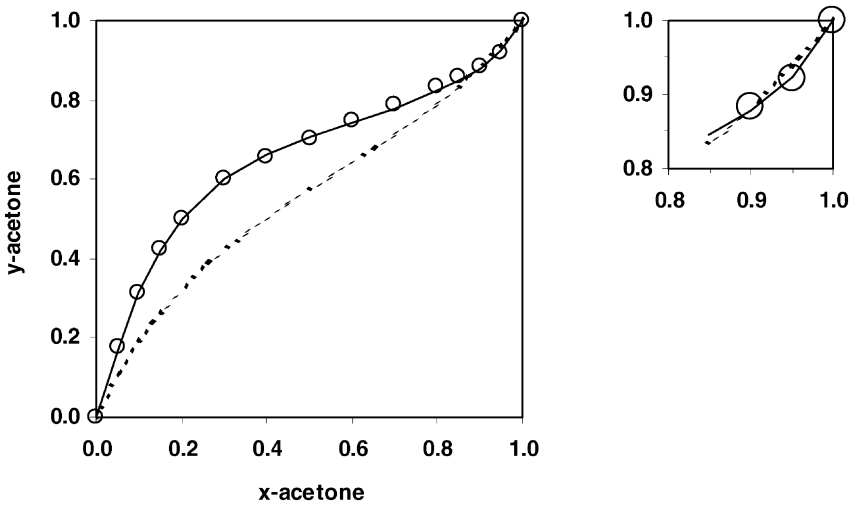

Fig. 9. VLE results for the $CaCl_2$–methanol–acetone system, saturated with respect to solid $CaCl_2$ at 1.0 atm. The salt-free equilibria are shown as a dashed line. Experimental data were taken from Ohe [53] and references cited therein. The lines were calculated using the model.

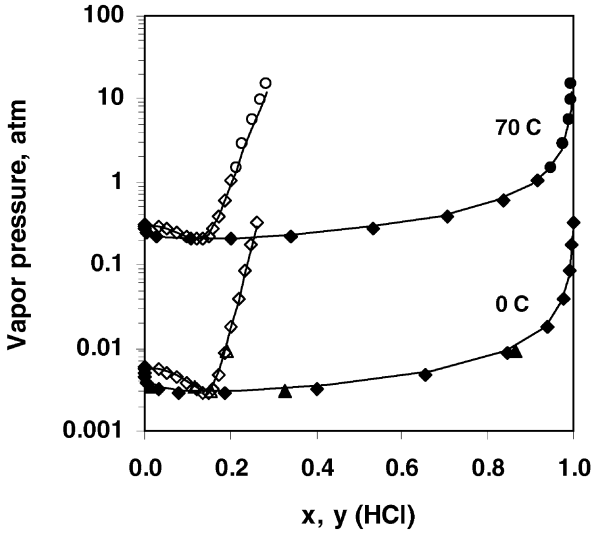

Fig. 10. VLE results for the HCl–water system at 0 and 70 °C. The experimental data were taken from Perry and Chilton [118] (◇ and ◆), Miller [119] (△ and ▲), and Kao [120] (○ and ●) and the lines were calculated from the model.

4.3.1. Acetic acid and formic acid

Acetic and formic acids are known to associate in aqueous solutions with the ionization constants of $10^{-4.76}$ for the acetic acid and $10^{-3.75}$ for the formic acid at 25 °C [69]. In mixed-solvents, these ionization constants change with the solvent composition [2,3]. The acids become more associated with an increase in the alcohol concentration and a decrease in the solvent dielectric constant. It is also well known that these acids are highly associated in the vapor phase to form dimers or higher polymers [70]. Realistic modeling of these systems must take into account the speciation reactions (i.e. ionization and dimerization) in both the liquid and the vapor phases. The ionization constants for formic acid and

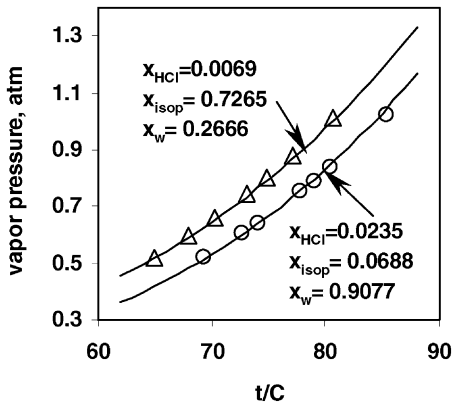

Fig. 11. VLE results for the HCl–water–isopropanol mixture as a function of temperature at fixed liquid compositions. The experimental data were taken from Ishidao et al. [121] and the lines were calculated from the model.

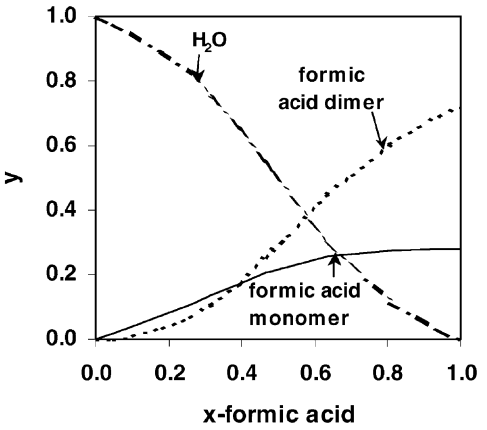

Fig. 12. Predicted vapor phase speciation in the formic acid–water system as a function of the mole fraction of formic acid at 60 °C.

acetic acid in water–alcohol mixtures such as water–methanol and water–ethanol have been reported in the literature [2,3]. Dimerization constants in the vapor phase for these acids are also available [70]. With these constants, the model can reproduce both VLE and chemical speciation in both liquid and vapor phases. The predicted vapor phase speciation is shown in Fig. 12. At the same time, the apparent dissociation constants of the acids in alcohol–water mixtures can also be reproduced. The results are shown in Fig. 13 for the ionization constants of formic acid and acetic acid in ethanol–water mixtures, and in Fig. 14 for the same acids in methanol–water mixtures.

When comparing the predicted speciation with the experimental apparent ionization constants, particular attention must be paid to the reference system that was used to report ionization constants [2,3]. The experimental ionization constants are usually reported on the mixed-solvent basis. For example, the

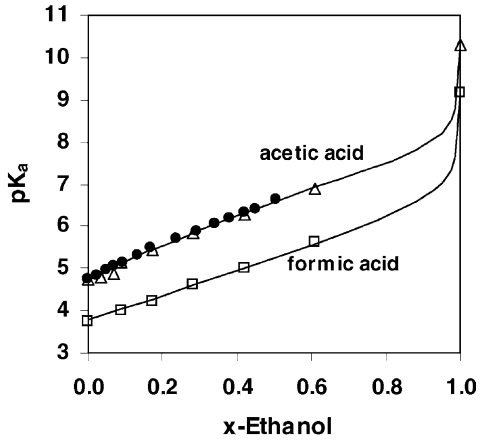

Fig. 13. Apparent ionization constants of acetic acid and formic acid in ethanol–water mixtures as a function of the ethanol mole fraction. The experimental data were taken from Panichajakul and Woolley [2] (filled symbols) and Sen et al. [3] (empty symbols).

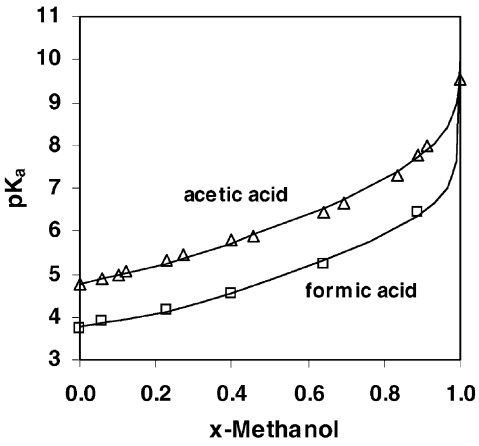

Fig. 14. Apparent ionization constants of acetic acid and formic acid in methanol–water mixtures as a function of the methanol mole fraction. The experimental data were taken from Sen et al. [3].

ionization constant of acetic acid in methanol–water mixtures is reported as

$$K_A = \frac{m_{H^+} m_{Ac^-}}{m_{HAc(aq)}} \frac{\gamma_{H^+} \gamma_{Ac^-}}{\gamma_{HAc(aq)}} \tag{38}$$

where m_i is the molality of species i in the mixed-solvent. At infinite dilution, this mixed-solvent-based ionization constant can be written as a function of the mole fractions of individual species:

$$K_A^* = \frac{1000 x_{H^+} x_{Ac^-}}{x_{HAc(aq)} (M_w x_w + M_m x_m)} \tag{39}$$

where M_w, x_w and M_m, x_m are the molecular weight and mole fraction of water and methanol, respectively. The value of K_A^* is different for each composition of the water–methanol mixture. However, the thermodynamic equilibrium constants for the acids, obtained from aqueous solutions, remain valid for all solvent compositions. By combining the aqueous-based thermodynamic equilibrium constants with the mixed-solvent activity coefficient model, the apparent ionization constants can be calculated according to Eq. (39). Additionally, Fig. 15 shows the predicted dissociation trend of acetic acid in ethanol–water mixtures at 25 °C.

4.3.2. Hydrogen fluoride

Another system that exhibits significant speciation effects is HF–water. This system is of considerable interest from the perspective of industrial applications such as glass etching, stainless steel pickling, aluminum refining, alkylation catalysis, and manufacture of fluorine-containing plastics. This is a particularly difficult system because of a very strong change in dissociation as a function of composition, coupled with multimerization of HF. Hydrogen fluoride is known to have a fairly low ionic dissociation in water ($pK_a = 3.45$) [69]. Electrical conductivity measurements in extremely anhydrous hydrogen fluoride also indicate a very low concentration of dissociated HF, i.e. $x_{F^-} \approx 3 \times 10^{-8}$ at 0 °C [71]. At the same time, strong multimerization of pure HF in both the liquid and gas states has been recognized by many authors [72,73]. The formation of dimers, hexamers and other products of self-association of HF in the vapor phase is well known and has been extensively investigated in the literature [74–77]. Infrared spectroscopic

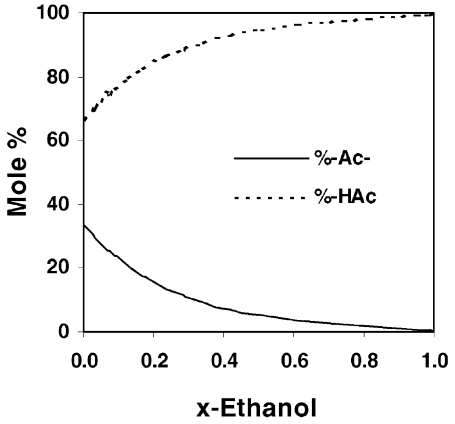

Fig. 15. Predicted dissociation trend of acetic acid in ethanol–water mixtures containing 10^{-4} mol HAc per 1 kg of solvent at 25 °C.

data seem to indicate the existence of monomers, dimers, trimers, and higher polymers [78,79]. Other studies have shown that *PVT* properties of the saturated HF vapor can be represented either by assuming only two molecular species, HF and H_6F_6 and a single equilibrium, $6HF(vap) = H_6F_6(vap)$ [75] or by assuming multiple association models [74]. The study of association of HF in the liquid phase is much less extensive. Although modeling studies yield the degree of association in the liquid phase [80–84], all these models are nonelectrolyte equations of state based on a combination of association theories with van der Waals-type equations. Thus, they impose a particular form of density dependence on association. However, there is no experimental indication whether these model results are valid. Polymerization of HF to hexamers in the liquid phase has also been indicated in experimental studies [85], but no quantitative data are given. In our treatment, we assumed only the monomer–hexamer equilibrium in the vapor phase, and used literature data for hexamerization constants [77]. In the liquid phase, the HF dissociation is constrained by the acid dissociation constant of HF in water, as determined using available experimental data [26,86], and by the low ionic concentrations in anhydrous HF derived from conductivity measurements [71]. Using vapor pressure data for the HF–water binary mixtures, and applying the constraints for the dissociation of HF, both phase equilibria and chemical speciation have been accurately reproduced over a wide temperature range and in the entire composition span as shown in Fig. 16. The speciation in the liquid phase and in the vapor phase in this system can be predicted as illustrated in Figs. 17 and 18 for 40 °C. To validate the speciation results, the predicted and experimental vapor phase compressibility factors have been compared. This comparison is shown in Fig. 19. The compressibility factor is a measure of the association of HF [75,81], as defined by Long et al. [75], i.e.

$$Z \cong \frac{n_T}{n_0} \tag{40}$$

where n_T is the total number of moles of all species in an associated mixture, and n_0 is the number of moles of all species that would exist in the absence of association. In our model for HF:

$$n_T = n_{monomer} + n_{hexamer} \tag{41}$$

$$n_0 = n_{monomer} + 6n_{hexamer} \tag{42}$$

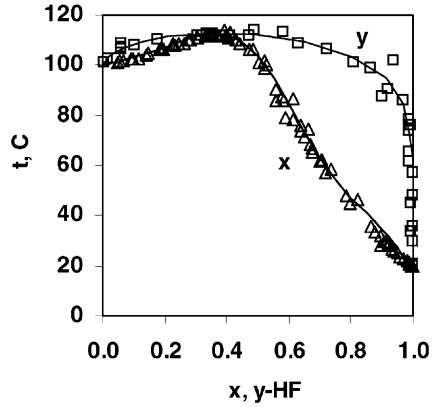

Fig. 16. VLE for HF–water at 1.0 atm. The experimental data were taken from the references cited in the TRC databank [51].

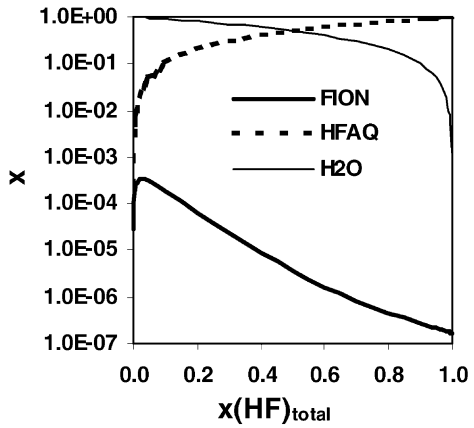

Fig. 17. Predicted liquid phase speciation in the HF–water system.

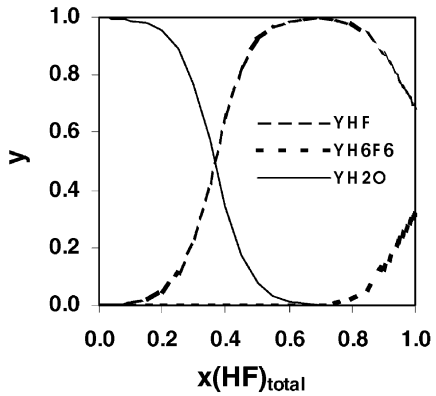

Fig. 18. Predicted vapor phase speciation in the HF–water system.

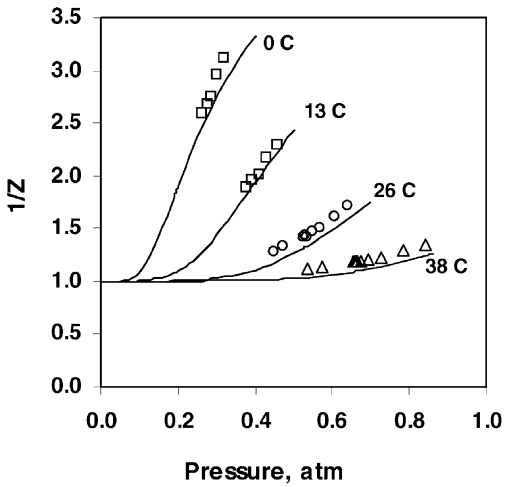

Fig. 19. The reciprocal of the vapor phase compressibility factor, 1/Z, of pure HF at various temperatures. The lines are predicted using the model and the experimental data are taken from Long et al. [75].

As shown in the figures, the present model can accurately represent the experimental results for vapor phase speciation. Because of a lack of direct experimental evidence of association in the liquid phase, a meaningful comparison can be made only for the gas phase.

4.3.3. Sulfuric acid

The thermodynamic treatment of sulfuric acid has been unusually difficult because of the change of the aqueous speciation ($H_2SO_4^0$, HSO_4^-, and SO_4^{2-}) with concentration, and the dissociation of the acid in the vapor phase to form sulfur trioxide ($H_2SO_4(g) = SO_3(g) + H_2O(g)$). An accurate model of the H_2SO_4–H_2O system is highly desirable due to the great practical importance of this system. Studies of the dissociation of aqueous H_2SO_4 have been reported in the literature [87–93]. For the dissociation of the bisulfate ion, the results from various authors are in fair agreement, at least at concentrations below 25m [94]. The results for the first dissociation of sulfuric acid ($H_2SO_4^0 = H^+ + HSO_4^-$), although quantitatively less consistent, all indicate a decrease in the dissociation with an increase in the sulfuric acid concentration. The interpretation of the Raman spectroscopic data of Rao [87] by Young and Blatz [88] indicates that a large fraction of the sulfuric acid is in the form of the associated $H_2SO_4^0$ neutral species at high sulfuric acid concentrations (e.g. ∼75% of sulfuric acid is associated to $H_2SO_4^0$ at $x_{H_2SO_4} \approx 0.4$, and ∼99% is associated in pure sulfuric acid at 25 °C). A later study by Young et al. [89] showed that the first dissociation of sulfuric acid in water is essentially complete, i.e. the bisulfate ions are the primary species at concentrations up to $x_{H_2SO_4} \approx 0.4$ at 25 °C. The dissociation decreases as the sulfuric acid concentration increases. The degree of association according to the reaction $H^+ + HSO_4^- = H_2SO_4^0$ becomes substantial as the sulfuric acid concentration further increases, and the association is nearly complete in pure sulfuric acid [89]. Raman spectroscopic data of Malinowski et al. [90] also show an increased relative concentration of $H_2SO_4^0$ as the sulfuric acid concentration increases from dilute to concentrated aqueous solutions. Similar results were obtained from the NMR measurements of Hood and Reilly [92].

Vapor–liquid equilibria for the H_2SO_4–H_2O system and the dissociation of H_2SO_4(g) in the vapor phase have been extensively studied [95–102]. The enthalpy of dilution and the heat capacities of aqueous sulfuric acid solutions are also reported over an extended concentration range [103–110]. The reported total pressures over sulfuric acid solutions from different authors are in fair agreement. The total vapor pressure and partial pressures of H_2O, SO_3, and H_2SO_4 have been calculated by Gmitro and Vermeulen [111] based on experimental VLE data over the concentration range of 10–100 wt.% of sulfuric acid and the experimentally determined equilibrium constants [96] for the dissociation of H_2SO_4(g) in the vapor phase. It has been pointed out that vapor pressure results in solutions with compositions approaching a pure acid are less accurate due to the very low vapor pressure, coupled with the dissociation of H_2SO_4(g) into H_2O(g) and SO_3(g) [97]. The vapor pressure of pure sulfuric acid as measured by different authors may differ by several hundred percent.

Due to the limited concentration range considered in most of the computational studies of aqueous sulfuric acid in the literature, the first dissociation of sulfuric acid was considered to be complete and only the dissociation of bisulfate ion was taken into account [91,94,112]. In the present work, both the first and the second dissociation of sulfuric acid have been taken into account in the liquid phase, together with the vapor phase dissociation of H_2SO_4(g). The results of VLE calculations show a very good agreement between the experimental and predicted total vapor pressure over the entire concentration range at various temperatures, as shown in Fig. 20. The calculated partial pressure behavior in the H_2SO_4–H_2O system is shown in Fig. 21 at 100 °C in the vicinity of the sulfuric acid azeotrope. The results are consistent with those obtained by Gmitro and Vermeulen [111].

4.4. Modeling density in mixed-solvent electrolyte solutions

Densities have been calculated for a number of systems that include aqueous electrolyte solutions, nonelectrolyte mixtures, and mixed-solvent electrolyte solutions. The results are shown in Fig. 22 for the

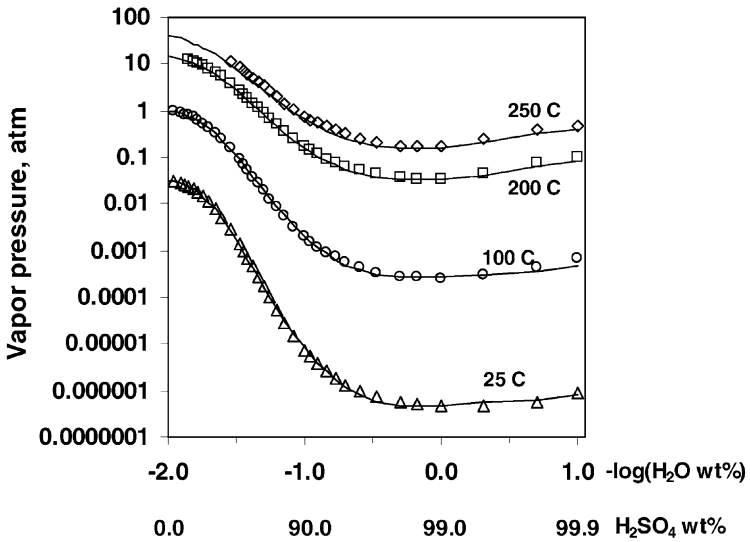

Fig. 20. VLE results for the H_2SO_4–H_2O system at various temperatures. The symbols are taken from the smoothed values of Gmitro and Vermeulen [111]. The lines are predicted using the model.

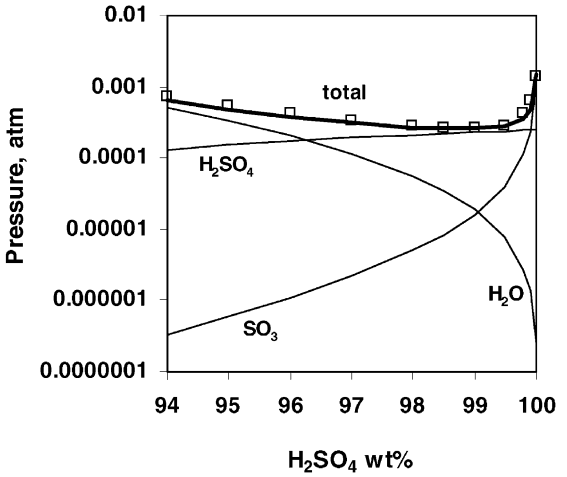

Fig. 21. The calculated partial pressures in the H_2SO_4–H_2O system at 100 °C in the vicinity of the sulfuric acid azeotrope. The symbols (total pressure) are taken from the smoothed values of Gmitro and Vermeulen [111].

NaOH–water system at various temperatures for solutions ranging from dilute to high concentrations. In Fig. 23, densities are shown for methanol–water mixtures at various temperatures. Finally, Fig. 24 shows the results for the NaCl–methanol–water system at 25 °C. As shown in these figures, good agreement between the calculated and experimental densities has been obtained.

4.5. Modeling the Gibbs energy of transfer

The experimental standard Gibbs energies of transfer have been included in the data regression to constrain the model so that the chemical potentials of species in a mixed-solvent can be correctly predicted in speciation calculations. Table 3 shows the calculated standard Gibbs energies of transfer for NaCl and

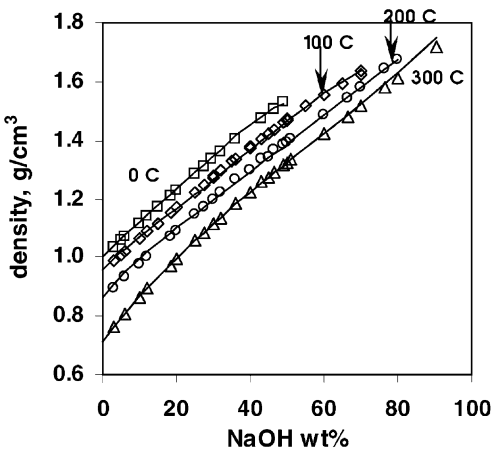

Fig. 22. Densities of the NaOH–water system at various temperatures and saturation pressures. The experimental data were taken from Söhnel and Novotnỳ [56], Dibrov et al. [122], Krumgal'z and Mashovets [123], and Krey [124].

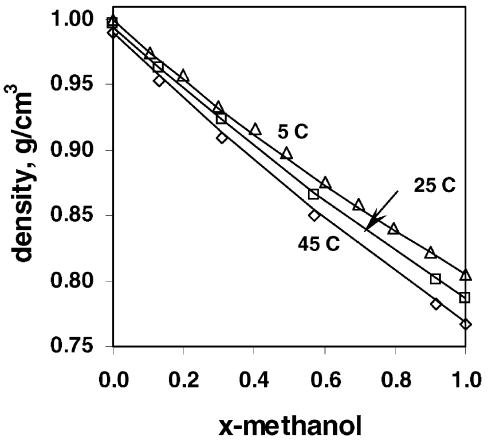

Fig. 23. Densities of the methanol–water system at various temperatures and at 1 atm. The experimental data were taken from Takenaka et al. (25 and 45 °C) [125a] and Easteal and Woolf (5 °C) [125b].

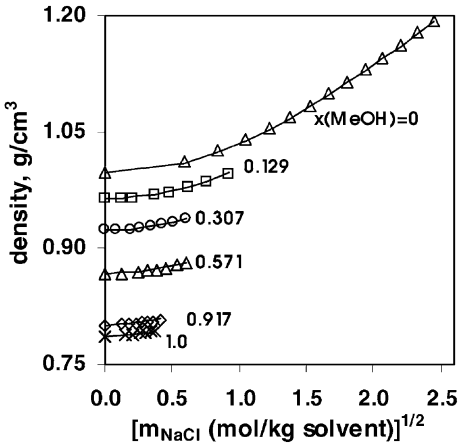

Fig. 24. Densities of the NaCl–methanol–water solutions at 25 °C and at various methanol concentrations. Experimental data were taken from Söhnel and Novotnỳ [56] for the data at $x_{\mathrm{MeOH}} = 0$ and from Takenaka et al. [125a] for other methanol concentrations.

Table 3
Calculated and experimental Gibbs energy of transfer for selected systems

Electrolyte	Solvents	$\Delta_{\mathrm{tr}}G_M$ (calculated, kJ mol^{-1})	$\Delta_{\mathrm{tr}}G_M$ (experimental, kJ mol^{-1})	$\Delta(\Delta_{\mathrm{tr}}G_M)$ (kJ mol^{-1})
LiCl	Water → ethanol	31.4	31	0.4
LiCl	Water → methanol	17.0	17	0.0
NaCl	Water → ethanol	35.7	34	1.7
NaCl	Water → methanol	20.3	21	−0.7

The experimental data were taken from Marcus [46].

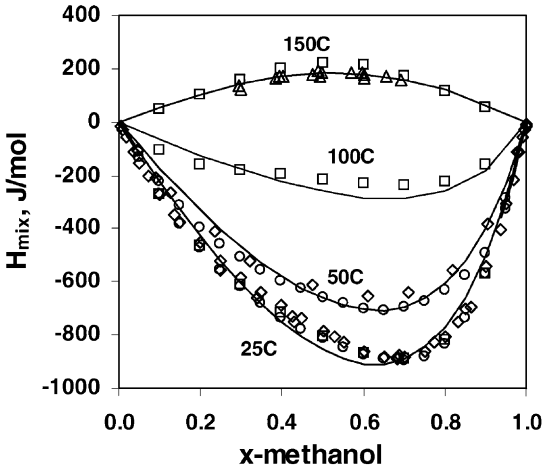

Fig. 25. Heats of mixing for methanol–water mixtures at various temperatures as a function of the methanol mole fraction. The experimental data were taken from Simonson et al. [126] (□), Wormald et al. [127] (△), Friese et al. [128] (○), and Christensen et al. [54] (◇).

LiCl from water to an organic solvent. The experimental data are also given for comparison. The model is capable of accurately reproducing the standard Gibbs energy of transfer data.

4.6. Modeling enthalpy and heat capacity

A thermodynamically consistent model should reproduce not only the properties that directly result from the excess Gibbs energy (i.e. VLE and SLE), but also the first and second derivatives of the Gibbs

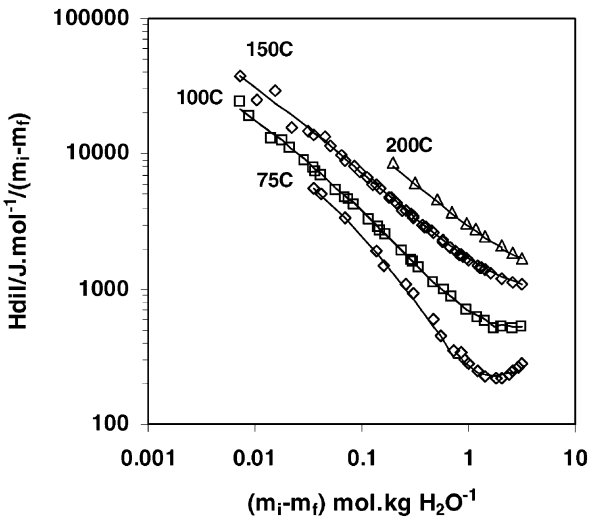

Fig. 26. Calculated and experimental heat of dilution data of aqueous NaCl at various temperatures at saturation pressures. The experimental data were taken from Mayrath and Wood [129].

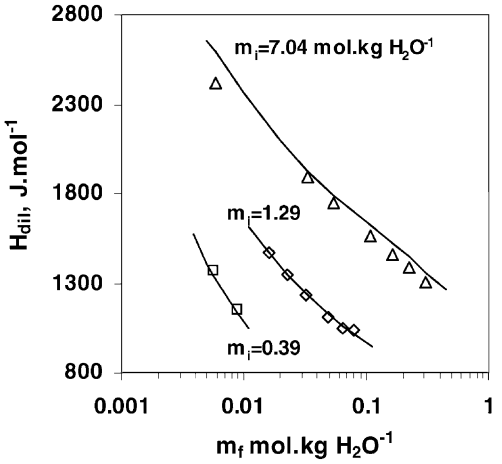

Fig. 27. Heats of dilution of aqueous citric acid at various initial concentrations and 25 °C. The experimental data were taken from Dobrogowska et al. [130].

energy with respect to temperature. Thus, heat of mixing and heat capacity data have been used, together with VLE and solubility data, to fit the model parameters so that consistent results can be obtained. Several types of enthalpy data have been considered, i.e.

1. heat of dilution (e.g. mixing aqueous single- or multi-salt solutions with water);
2. heat of mixing of two pure components (e.g. methanol with water);
3. heat of mixing of a solution of a salt in one solvent with another, less polar, pure solvent (e.g. mixing an aqueous NaCl solution with methanol).

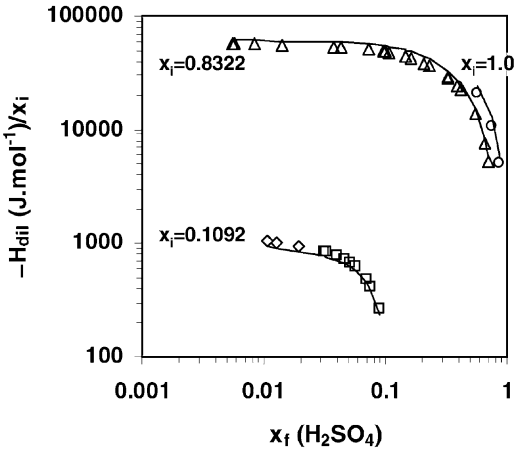

Fig. 28. Calculated and experimental heats of dilution of aqueous H_2SO_4 as a function of $x_{f(H_2SO_4)}$ at various initial H_2SO_4 mole fractions at 40 °C. The experimental data were taken from Kim and Roth [131] (△, ○, ◇) and Rutten et al. [132] (□).

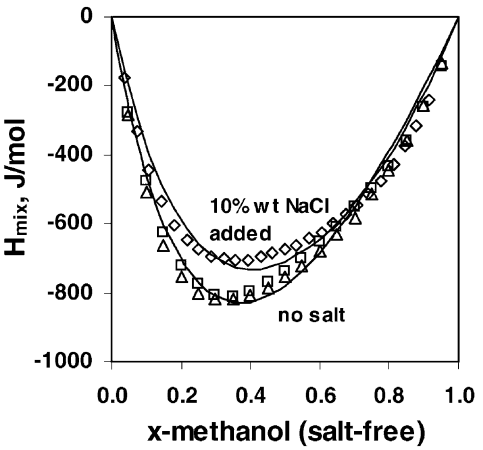

Fig. 29. Calculated and experimental heats of mixing of methanol with an aqueous solution of NaCl (10 wt.%, upper curve) and with pure water (lower curve) at 35 °C. The experimental data were taken from Friese et al. [128] for the salt effects (◇) and from Friese et al. [128] (△) and Christensen et al. [54] (□) for other points.

Fig. 25 shows the heat of mixing for methanol–water mixtures at various temperatures. The heats of dilution of aqueous NaCl and citric acid solutions are shown in Figs. 26 and 27, respectively. Heats of dilution for various initial concentrations of sulfuric acid including anhydrous H_2SO_4 ($x_i = 1$) are shown in Fig. 28. It is of particular interest to examine how the model predicts the effects of a salt on the heat of mixing of two solvents. Fig. 29 shows the results when an aqueous NaCl solution is mixed with pure methanol. The heats of mixing of salt-free water with methanol are also shown in the figure. Heat capacities are shown in Figs. 30 and 31 for sulfuric acid solutions in the entire concentration range and for aqueous NaCl solutions at different temperatures. These results indicate that the model can accurately represent heats of dilution and mixing and heat capacities in mixed-solvent electrolyte solutions of various types.

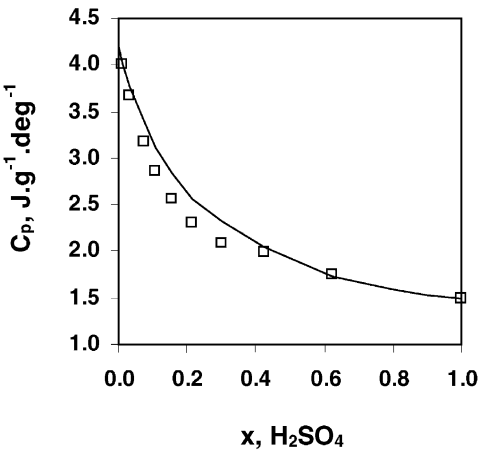

Fig. 30. Heat capacities of sulfuric acid solutions in the entire concentration range at 80 °C. The symbols are the literature data taken from Zaytsev and Aseyev [103] and the lines were calculated from the model.

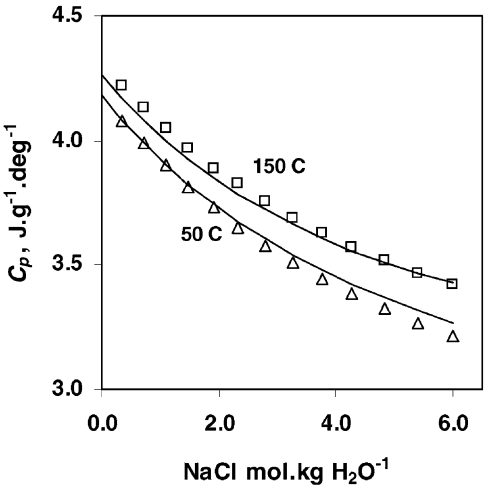

Fig. 31. Heat capacities of aqueous NaCl solutions as a function of NaCl molality at 50 and 150 °C. The symbols denote literature data taken from Zaytsev and Aseyev [103] and the lines were calculated from the model.

5. Conclusions

A new, comprehensive thermodynamic model for mixed-solvent electrolyte systems has been developed for the simultaneous calculation of speciation, phase equilibria, enthalpies, heat capacities, and densities. The model contains three contributions to the excess Gibbs energy: a long-range electrostatic interaction term represented by the Pitzer–Debye–Hückel expression, a short-range interaction term expressed by the UNIQUAC model for binary interactions between all species, and a middle-range term of a second virial coefficient-type for the remaining ionic interactions. The solution chemistry is modeled by incorporating explicit speciation calculations so that all chemical equilibria of ionic dissociation, ion pair formation, hydrolysis of metal ions, formation of metal–ligand complexes, acid–base reactions, etc. are taken into account. The model has been designed to encompass systems containing electrolytes and nonelectrolytes with any composition. The speciation calculations rely on the use of the Helgeson–Kirkham–Flowers equation of state, coupled with extensive databases of standard-state properties of aqueous species. Special attention has been paid to ensuring thermodynamic consistency when the standard-state properties are combined with activity coefficients. In addition, the model has been constrained to represent the Gibbs energy of transfer between solvents so that the chemical potentials of species are correctly reproduced. Furthermore, a methodology has been developed to constrain the model to reproduce heat capacities and densities of both pure components and mixtures. The model has been extensively validated using experimental data for VLE, solubility, activity coefficients, acid dissociation constants in mixed-solvents, speciation, Gibbs energy of transfer, density, heats of mixing and dilution, and heat capacity. The model is valid for a wide class of electrolyte systems including aqueous electrolyte solutions ranging from infinite dilution to fused salts, fully miscible acids, electrolytes in organic and mixed-solvents, and nonelectrolyte mixtures. For all types of systems and data, the model has been shown to reproduce experimental results with good accuracy.

List of symbols

a_{ij}	UNIQUAC interaction parameter between i and j
$a_{ij}^{(0)}, a_{ij}^{(1)}, a_{ij}^{(2)}$	UNIQUAC parameters in activity coefficient calculations
$a_{ij}^{(3)}, a_{ij}^{(4)}, a_{ij}^{(5)}$	UNIQUAC parameters in density calculations
A_x	Debye–Hückel parameter, defined in Eq. (8)
$b_{ij}, c_{ij}, d_{ij}, e_{ij}, f_{ij}$	middle-range parameters in activity coefficient calculations
$b'_{ij}, c'_{ij}, d'_{ij}, e'_{ij}, f'_{ij}, g'_{ij}, h'_{ij}$	middle-range parameters in density calculations
B_{ij}	middle-range interaction parameter between i and j
$C^0_{p,i}$	molar heat capacity of pure liquid i
G^{ex}	excess Gibbs free energy
$\Delta_{\mathrm{tr}}G^{\circ}_i$	Gibbs energy of transfer of i
h	molar enthalpy
h^{ex}	excess molar enthalpy of a mixture
$h^{\mathrm{ex},*}$	excess molar enthalpy of a mixture in the unsymmetrical convention
h^0_i	molar enthalpy of pure liquid i
h^*_i	standard-state partial molar enthalpy of i
I_x	mole fraction-based ionic strength, defined in Eq. (7)
K_{A}	ionization constant
m_i	molality of i
M_i	molecular weight of i
n_i	number of moles of i
P	pressure (MPa)
q_i	UNIQUAC surface area parameter
r_i	UNIQUAC size parameter
T	temperature (K)
$v^{\mathrm{ex},*}$	excess molar volume of a mixture in the unsymmetrical convention
v^0_i	molar volume of pure liquid i
v^*_i	standard-state partial molar volume of i
x_i	mole fraction of i
Z	compressibility factor

Greek symbols

γ_i	activity coefficient of i
γ^*_i	activity coefficient of species i in unsymmetrical convention
μ^0_i	standard-state chemical potential of species i
$\mu^{*,x,0}_i$	standard-state chemical potential of species i in unsymmetrical reference state and mole fraction convention
$\mu^{*,m,0}_i$	standard-state chemical potential of species i in unsymmetrical reference state and molality convention
ρ	density

Acknowledgements

This work was supported by the Department of Energy under the Cooperative Agreement No. DE-FC02-00CH11019 and co-sponsored by Dow Chemical, DuPont, Westvaco and Materials Technology Institute. The authors acknowledge the assistance of Ronald Springer in testing the model.

References

[1] A. Anderko, P. Wang, M. Rafal, Fluid Phase Equilib. 194–197 (2002) 123–142.
[2] C.C. Panichajakul, E.M. Woolley, in: W.F. Furter (Ed.), Thermodynamic Behavior of Electrolytes in Mixed Solvents, Advances in Chemistry Series 155, American Chemical Society, Washington, DC, 1976.
[3] B. Sen, R.N. Roy, J.J. Gibbons, D.A. Johnson, L.H. Adcock, in: W.F. Furter (Ed.), Thermodynamic Behavior of Electrolytes in Mixed Solvents. II. Advances in Chemistry Series 177, American Chemical Society, Washington, DC, 1979.
[4] P. Debye, E. Hückel, Phys. Z. 24 (1924) 185.
[5] R.A. Robinson, R.H. Stokes, Electrolyte Solutions, 2nd Edition, Butterworths, London, 1959.
[6] J.M. Prausnitz, R.N. Lichtenthaler, E.G. de Azevedo, Molecular Thermodynamics of Fluid-Phase Equilibria, 2nd Edition, Prentice-Hall, Englewood Cliffs, NJ, 1986.
[7] W.E. Acree Jr., Thermodynamic Properties of Nonelectrolyte Solutions, Academic Press, New York, 1984.
[8] M. Rafal, J.W. Berthold, N.C. Scrivner, S.L. Grise, Models for electrolyte solutions, in: S.I. Sandler (Ed.), Models for Thermodynamic and Phase Equilibria Calculations, Marcel Dekker, New York, 1994, p. 601.
[9] B. Sander, A. Fredenslund, P. Rasmussen, Chem. Eng. Sci. 41 (1986) 1171–1183.
[10] E.A. Macedo, P. Skovborg, P. Rasmussen, Chem. Eng. Sci. 45 (1990) 875–882.
[11] I. Kikic, M. Fermeglia, P. Rasmussen, Chem. Eng. Sci. 46 (1991) 2775–2780.
[12] J. Li, H.-M. Polka, J. Gmehling, Fluid Phase Equilib. 94 (1994) 89–114.
[13] H. Zerres, J.M. Prausnitz, AIChE J. 40 (1994) 676–691.
[14] W. Yan, M. Topphoff, C. Rose, J. Gmehling, Fluid Phase Equilib. 162 (1999) 97–113.
[15] Y. Liu, S. Watanasiri, Fluid Phase Equilib. 116 (1996) 193–200.
[16] M.C. Iliuta, K. Thomsen, P. Rasmussen, Chem. Eng. Sci. 55 (2000) 2673–2686.
[17] A. Kolker, J.J. de Pablo, Ind. Eng. Chem. Res. 35 (1996) 228–233.
[18] S. Dahl, E.A. Macedo, Ind. Eng. Chem. Res. 31 (1992) 1195–1201.
[19] B. Mock, L.B. Evans, C.-C. Chen, AIChE J. 32 (1986) 1655–1664.
[20] M.J.E. De M. Cardoso, J.P. O'Connell, Fluid Phase Equilib. 33 (1987) 315–326.
[21] J.Y. Zuo, D. Zhang, W. Fürst, AIChE J. 46 (2000) 2318–2329.
[22] H.C. Helgeson, D.H. Kirkham, Am. J. Sci. 274 (1974) 1089–1198.
[23] H.C. Helgeson, D.H. Kirkham, Am. J. Sci. 274 (1974) 1199–1261.
[24] H.C. Helgeson, D.H. Kirkham, Am. J. Sci. 276 (1976) 97–240.
[25] H.C. Helgeson, D.H. Kirkham, G.C. Flowers, Am. J. Sci. 281 (1981) 1241–1516.
[26] E.L. Shock, H.C. Helgeson, D.A. Sverjensky, Geochim. Cosmochim. Acta 53 (1989) 2157–2183.
[27] E.L. Shock, H.C. Helgeson, Geochim. Cosmochim. Acta 52 (1988) 2009–2036.
[28] E.L. Shock, D.C. Sassani, M. Willis, D.A. Sverjensky, Geochim. Cosmochim. Acta 61 (1997) 907–950.
[29] D.A. Sverjensky, E.L. Shock, H.C. Helgeson, Geochim. Cosmochim. Acta 61 (1997) 1359–1412.
[30] E.L. Shock, H.C. Helgeson, Geochim. Cosmochim. Acta 54 (1990) 915–945.
[31] S. Malanowski, A. Anderko, Modeling Phase Equilibria. Thermodynamic Background and Practical Tools, Wiley Series in Chemical Engineering, Wiley, New York, 1992.
[32] K.S. Pitzer, J. Phys. Chem. 77 (1973) 268–277.
[33] K.S. Pitzer, J. Am. Chem. Soc. 102 (1980) 2902–2906.
[34] K.S. Pitzer, J.M. Simonson, J. Phys. Chem. 90 (1986) 3005–3009.
[35] C.-C. Chen, H.I. Britt, J.F. Boston, L.B. Evans, AIChE J. 28 (1982) 588–596.
[36] C.-C. Chen, L.B. Evans, AIChE J. 32 (1986) 444–454.
[37] C. Achard, C.-G. Dussap, J.-B. Gros, AIChE J. 40 (1994) 1210–1222.

[38] C. Achard, C.-G. Dussap, J.-B. Gros, Fluid Phase Equilib. 98 (1994) 71–89.
[39] S.P. Pinho, E.A. Macedo, Fluid Phase Equilib. 116 (1996) 209–216.
[40] S.L. Clegg, K.S. Pitzer, P. Brimblecombe, J. Phys. Chem. 96 (1992) 9470–9479.
[41] Y.Y. Akhadov, Dielectric Properties of Binary Solutions, Pergamon Press, New York, 1980.
[42] P. Wang, A. Anderko, Fluid Phase Equilib. 186 (2001) 103–122.
[43] T.C. Tan, Chem. Eng. Res. Des. 65 (1987) 355–366;
T.C. Tan, Chem. Eng. Res. Des. 68 (1990) 93–103.
[44] D.S. Abrams, J.M. Prausnitz, AIChE J. 21 (1975) 116–128.
[45] L.-J.B. Lee, Dissertation, University of Oklahoma, 1996.
[46] Y. Marcus, Ion Properties, Marcel Dekker, New York, 1997.
[47] T.E. Daubert, R.P. Danner, Physical and Thermodynamic Properties of Pure Chemicals. Data Compilation, Hemisphere, New York, 1989.
[48] W. Linke, A. Seidell, Solubilities of Inorganic and Metal-Organic Compounds, Vols. 1 and 2, American Chemical Society, Washington, DC, 1965.
[49] H. Stephen, T. Stephen, Solubilities of Inorganic and Organic Compounds, Vols. 1 and 2, Pergamon Press, New York, 1979.
[50] H.L. Silcock, Solubilities of Inorganic and Organic Compounds, Vol. 3, Pergamon Press, New York, 1979.
[51] A. Maczynski, A. Skrzecz, TRC Data Bases for Chemical and Engineering. Floppy Books on VLE, LLE and SLE, 1995–1999.
[52] J. Gmehling, U. Onken, Vapor–Liquid Equilibrium Data Collection. Dechema Chemistry Data Series, 1977.
[53] S. Ohe, Vapor–Liquid Equilibrium Data—Salt Effect. Physical Sciences Data Series, No. 43, Elsevier, New York, 1991.
[54] J.J. Christensen, R.W. Hanks, R.M. Izatt, Handbook of Heats of Mixing, Wiley, New York, 1982.
[55] Y.P. Handa, G.C. Benson, Fluid Phase Equilib. 3 (1979) 185–249.
[56] O. Söhnel, P. Novotnỳ, Densities of Aqueous Solutions of Inorganic Substances. Physical Sciences Data 22, Elsevier, New York, 1985.
[57] A. Bondi, Physical Properties of Molecular Crystals, Liquids, and Glasses, Wiley, New York, 1968.
[58] M.-C. Trudelle, M. Abraham, Can. J. Chem. 55 (1977) 1713–1719.
[59] T.B. Tripp, J. Chem. Thermodyn. 7 (1975) 263–269.
[60] T.B. Tripp, J. Braunstein, J. Phys. Chem. 73 (1969) 1984–1990.
[61] H.F. Gibbard, G. Scatchard, J. Chem. Eng. Data 18 (1973) 293–298.
[62] T.H. Braunstein, J. Braunstein, J. Chem. Thermodyn. 3 (1971) 419–431.
[63] J.M. Simonson, K.S. Pitzer, J. Phys. Chem. 90 (1986) 3009–3013.
[64] M. Spankar, J.B. Macaskill, R.G. Bates, J. Solution Chem. 8 (1979) 887–895.
[65] M.A. Esteso, O.M. Gonzalez-Diaz, F.F. Hernandez-Lius, L. Fernandez-Merida, J. Solution Chem. 18 (1989) 277–288.
[66] A.J. Dill, L.M. Itzkowitz, O. Popovych, J. Phys. Chem. 72 (1968) 4580–4586.
[67] P. Longhi, P.R. Mussini, T. Mussini, S. Rondinini, J. Solution Chem. 17 (1988) 417–427.
[68] (a) P.D. Ceccattini, P.R. Mussini, T. Mussini, J. Solution Chem. 26 (1997) 1169–1186;
(b) J. Murto, Acta Chem. Scand. 18 (1964) 1043–1053.
[69] R.W. Weast, D. Lide, CRC Handbook of Chemical Physics, 70th Edition, CRC Press, Boca Raton, FL, 1990.
[70] A. Ksiazczak, A. Anderko, Ber. Bunsenges. Phys. Chem. 92 (1988) 496–504.
[71] N. Miki, M. Maeno, T. Ohmi, J. Electrochem. Soc. 137 (1990) 790–794.
[72] J.H. Simons, Fluorine Chemistry, Vol. I, Academic Press, New York, NY, 1950.
[73] Kirk-Othmer Encyclopedia of Chemical Technology, Vol. 10, 1980, pp. 733–753.
[74] J.M. Beckerdite, D.R. Powell, E.T. Adams Jr., J. Chem. Eng. Data 28 (1983) 287–293.
[75] R.W. Long, J.H. Hildebrand, W.E. Morrell, J. Am. Chem. Soc. 65 (1943) 182–187.
[76] C.E. Vanderzee, W.W.M. Rodenburg, J. Chem. Thermodyn. 2 (1970) 461–478.
[77] W. Schotte, Ind. Eng. Chem. Process Dev. 19 (1980) 432–439.
[78] D.F. Smith, J. Chem. Phys. 28 (1958) 1040–1056.
[79] J.L. Hollenberg, J. Chem. Phys. 46 (1967) 3271–3273.
[80] M.M. Lencka, A. Anderko, AIChE J. 39 (1993) 533–538.
[81] A. Anderko, J.M. Prausnitz, Fluid Phase Equilib. 95 (1994) 59–71.
[82] C.H. Twu, J.E. Coon, J.R. Cunningham, Fluid Phase Equilib. 86 (1993) 47–62.

[83] C.P.A. Kao, M.L. Paulaitis, Fluid Phase Equilib. 108 (1995) 27–46.
[84] D.P. Visco, D.A. Kofke, Ind. Eng. Chem. Res. 38 (1999) 4125.
[85] J.H. Simons, J.W. Bouknight, J. Am. Chem. Soc. 54 (1932) 129–135.
[86] C.K. Richardson, H.D. Holland, Geochim. Cosmochim. Acta 43 (1979) 1313–1325.
[87] N.R. Rao, Indian J. Phys. 14 (1940) 143.
[88] T.F. Young, L.A. Blatz, Chem. Rev. 44 (1949) 93–115.
[89] T.F. Young, L.F. Maranville, H.M. Smith, in: W.J. Hamer (Ed.), The Structure of Electrolytic Solutions, Wiley, New York, 1959.
[90] E.R. Malinowski, R.A. Cox, U.L. Haldna, Anal. Chem. 56 (1984) 778–781.
[91] S.L. Clegg, P. Brimblecombe, J. Chem. Eng. Data 40 (1995) 43–64.
[92] G.C. Hood, C.A. Reilly, J. Chem. Phys. 27 (1957) 1126–1128.
[93] G.E. Walrafen, W.-H. Yang, Y.C. Chu, M.S. Hokmabadi, J. Solution Chem. 29 (2000) 905–936.
[94] S.L. Clegg, J.A. Rard, K.S. Pitzer, J. Chem. Soc., Faraday Trans. 90 (1994) 1875–1894.
[95] E. Abel, J. Phys. Chem. 50 (1946) 260–283.
[96] M. Bodenstein, M. Katayama, Z. Electrochem. 15 (1909) 244–249.
[97] P. Bolsaitis, J.F. Elliott, J. Chem. Eng. Data 35 (1990) 69–85.
[98] G.H. Greenwalt, Ind. Eng. Chem. 17 (1925) 522–523.
[99] S. Shankman, A.R. Gordon, J. Am. Chem. Soc. 61 (1939) 2370–2373.
[100] R. Haase, H.-W. Borgmann, Korrosion 15 (1960) 47–49.
[101] E.M. Collins, J. Phys. Chem. 37 (1933) 1191–1203.
[102] B.G. Staples, J.M. Procopio Jr., G.J. Su, Chem. Eng. November 16 (1970) 113–115.
[103] I.D. Zaytsev, G.G. Aseyev, Properties of Aqueous Solutions of Electrolytes, CRC Press, Boca Raton, FL, 1992.
[104] E. Lange, J. Monheim, A.L. Robinson, J. Am. Chem. Soc. 55 (1933) 4733–4744.
[105] Y.C. Wu, T.F. Young, J. Res. Natl. Bur. Stand. 85 (1980) 11–17.
[106] P. Rutten, S.H. Kim, M. Roth, Fluid Phase Equilib. 153 (1998) 317–340.
[107] S.H. Kim, M. Roth, J. Chem. Eng. Data 46 (2001) 138–143.
[108] J.E. Kunzler, W.F. Giauque, J. Am. Chem. Soc. 74 (1952) 3472–3476.
[109] D.N. Craig, G.W. Vinal, J. Res. Natl. Bur. Stand. 24 (1940) 475–490.
[110] W.F. Giauque, E.W. Hornung, J.E. Kunzler, T.R. Rubin, J. Am. Chem. Soc. 82 (1960) 62–70.
[111] J.I. Gmitro, T. Vermeulen, AIChE J. 10 (1964) 740–746.
[112] M. Cherif, A. Mgaidi, M.N. Ammar, M. Abderrabba, W. Fürst, Fluid Phase Equilib. 194–197 (2002) 729–738.
[113] F.P. Hoffmann, W. Viogt, ELDATA: Int. Electron J. Phys.-Chem. Data 2 (1996) 31–36.
[114] D. Garvin, V.B. Parker, H.J. White Jr., CODATA Thermodynamic Tables. Selections for Some Compounds of Calcium and Related Mixtures: A Prototype Set of Tables, Hemisphere, Washington, DC, 1987.
[115] E.R. Signit, H.D. Holland, C.J. Biscardi, Geochim. Cosmochim. Acta 26 (1962) 1301–1331.
[116] A.J. Ellis, Am. J. Sci. 261 (1963) 259–267.
[117] D.G. Archer, J. Phys. Chem. Ref. Data 21 (1992) 793–829.
[118] R.H. Perry, C.H. Chilton, Chemical Engineers' Handbook, 5th Edition, McGraw-Hill, New York, 1973.
[119] E. Miller, J. Chem. Eng. Data 28 (1983) 363.
[120] J.T.F. Kao, J. Chem. Eng. Data 15 (1970) 362–367.
[121] T. Ishidao, Y. Iwai, Y. Arai, K. Ochi, T. Yamamura, T. Ishikawa, Fluid Phase Equilib. 178 (2001) 239–257.
[122] A. Dibrov, V.P. Mashovets, R.P. Matveeva, J. Appl. Chem. USSR (Eng. Trans.) 37 (1964) 38–44.
[123] B.S. Krumgal'z, V.P. Mashovets, J. Appl. Chem. USSR (Eng. Trans.) 37 (1964) 2563–2566.
[124] J. Krey, Z. Phys. Chem. Neue Folge 81 (1974) 252–273.
[125] (a) N. Takenaka, T. Takemura, M. Sakurai, J. Chem. Eng. Data 39 (1994) 207–213;
(b) A.J. Easteal, L.A. Woolf, J. Chem. Thermodyn. 17 (1985) 49–62.
[126] J.M. Simonson, D.J. Bradley, R.H. Busey, J. Chem. Thermodyn. 19 (1987) 479–492.
[127] C.J. Wormald, L. Badock, M.J. Lloyd, J. Chem. Thermodyn. 28 (1996) 603–613.
[128] T. Friese, P. Ulbig, S. Schulz, K. Wagner, J. Chem. Eng. Data 44 (1999) 701–714.
[129] J.E. Mayrath, R.H. Wood, J. Chem. Thermodyn. 14 (1982) 15–26.
[130] C. Dobrogowska, L.G. Hepler, A. Apelblat, J. Chem. Thermodyn. 22 (1990) 167–172.
[131] S.H. Kim, M. Roth, J. Chem. Eng. Data 46 (2001) 138–143.
[132] P. Rutten, S.H. Kim, M. Roth, Fluid Phase Equilib. 153 (1998) 317–340.
[133] J.-L. Fortier, P.-A. Leduc, J.E. Desnoyers, J. Solution Chem. 3 (1974) 323–349.
[134] W.H. Leung, F.J. Millero, J. Solution Chem. 4 (1975) 145–159.